https://doi.org/10.5194/egusphere-2026-3544
Preprint. Discussion started: 9 July 2026

Impacts of record Antarctic sea ice losses in 2022–2023 on swell-induced flexure of ice shelves

Nathan J. Teder[1], Luke G. Bennetts[1], Phillip A. Reid[2, 3], and Robert A. Massom[4,3,5]

[1]The University of Melbourne, Parkville, Victoria, Australia
[2]Australian Bureau of Meteorology, Hobart, Tasmania, Australia
[3]Australian Antarctic Program Partnership, Hobart, Tasmania, Australia
[4]Australian Antarctic Division, Hobart, Tasmania, Australia
[5]Australian Centre for Excellence in Antarctic Sciences (ACEAS), Institute for Marine and Antarctic Studies, University of Tasmania, Hobart, Tasmania

Correspondence: Nathan J. Teder (nathan.teder@outlook.com)

Abstract

Recent case studies have highlighted regional loss of Antarctic sea ice triggering large-scale ice shelf calving events, by allowing damaging ocean swell to reach shelf fronts. Thus, the dramatic and widespread loss of Antarctic sea ice in recent years has implications for the stability of ice shelves. Here, observations and models are used to conduct a broad assessment of changes in swell-induced flexural stress levels experienced by Antarctic ice shelves, with a focus on the record sea-ice lows of 2022 and 2023. Daily time series are constructed for effective lengths of the sea-ice barriers protecting fourteen Antarctic ice shelves, and for the incoming swell, along with yearly values for shelf front thickness, over a decade leading up to and including 2022–2023. The flexural stress levels are generally found to be far greater in 2022 and 2023 than the preceding eight years, and this is shown to be primarily driven by sea-ice loss, although sometimes mitigated by reduced peak periods of incoming swell. Further, it is shown that flexural stress anomalies are strongly correlated with anomalies in effective sea-ice length and peak period, and that an increase or decrease in flexural stress can be predicted by relative changes in sea-ice length and peak period. The findings indicate that more Antarctic ice shelves will become susceptible to enhanced swell-induced flexural stress if sea-ice losses and ice shelf thinning continue. Under these scenarios, predictions are made of when flexural stress will become a dominant contributor to total ice shelf stress for each of the fourteen ice shelves studied.

1 Introduction

Approximately a decade ago, overall Antarctic sea ice extent was baffling scientists by breaking records in its maximum extent, despite warming temperatures (Gulev et al., 2021; Reid and Massom, 2015; Reid et al., 2015; Parkinson, 2019). Shortly after setting its record maximum extent in September 2014, Antarctic sea ice began to retreat and repeatedly broke its record

https://doi.org/10.5194/egusphere-2026-3544
Preprint. Discussion started: 9 July 2026

minimum extent (Parkinson, 2019; Eayrs et al., 2021; Turner et al., 2022; Gilbert and Holmes, 2024). The minima are a signal of Antarctic sea ice switching to a new state, which is characterised by consistent negative anomalies in circumpolar sea ice extent (Purich and Doddridge, 2023; Hobbs et al., 2024). Sea ice losses were most pronounced and widespread around Antarctica in 2022 and 2023 (Fig. 1a,b; Schroeter et al., 2023; Reid et al., 2024).

Farther south, approximately three quarters of the Antarctic Ice Sheet's grounded ice boundary abuts ice shelves or outlet glaciers, which provide a buttressing effect to slow the outflow of the Antarctic Ice Sheet into the Southern Ocean and, hence, moderate sea level rise (Bindschadler et al., 2011; Gudmundsson, 2013; Fürst et al., 2016; Noble et al., 2020). Over recent decades, many Antarctic ice shelves have been losing mass through a combination of thinning (melting) and shelf front retreat (calving). Calving is responsible for roughly half of the total Antarctic ice shelf mass loss since 1997 ($\approx$ 6,000 GT Greene et al., 2022; Davison et al., 2023), and the frequency of calving events has increased in recent years, going from 69–127 calving events per year in 2005–2016, to 168–225 events per year from 2016–2020 (Qi et al., 2021).

From 2000–2019, the increased calving rate of Antarctic ice shelves has been positively correlated with reduced sea ice extent in Austral summer (Doddridge et al., 2025). The correlation is attributed to the role sea ice has in modulating the levels and modes of ice shelf stress responsible for the fracture amplification and rift propagation that result in calving events. In addition to providing a backstress that reduces internal ice shelf stress (Gomez-Fell et al., 2022; Provost et al., 2024; Walker et al., 2024; Bassis et al., 2024), sea ice, in the form of both stationary consolidated face ice and moving pack ice, creates a barrier that attenuates potentially damaging ocean swell before they reaches an ice shelf (Massom et al., 2010; Baker et al., 2019; Squire, 2020; Bennetts et al., 2024a). Swell that reaches an ice shelf is partially reflected by the shelf front and partially transmitted into the ice shelf and sub-shelf water cavity region (Meylan et al., 2021; Bennetts et al., 2024b). The transmitted swell imparts flexural stress on the shelf front region (Banwell et al., 2017; Lipovsky, 2018), and sustained periods of sea ice loss and swell reaching ice shelves have been connected with large-scale calving and ice shelf disintegration events (Massom et al., 2018; Teder et al., 2025). Thinner shelf fronts allow greater transmission of swell, which implies a connection between thinning and shelf-front retreat through the swell-induced calving process (Teder et al., 2025).

The dramatic and widespread Antarctic sea ice losses in 2022 and 2023 are likely to have substantially increased the levels of flexural stress imposed by swell on ice shelves around Antarctica. In this paper, we construct a yearly dataset of shelf front thickness, and daily datasets on sea-ice barrier length and incoming swell, for ten years leading up to and including 2022 and 2023, for 14 major Antarctic ice shelves (Fig. 1a). These ice shelves cover both East and West Antarctica and were chosen due to both size and potential future impact should they recede. We combine these datasets in a model to generate daily flexural stress time series for each ice shelf. We assess the increases in flexural stress during the sea ice lows of 2022 and 2023 in comparison to the preceding eight years, in which the minimum sea ice extents were greater than 2×10^6 km^2, and we conduct a statistical analysis to determine the driving factors for the flexural stress increases. We conclude the study by considering future scenarios that highlight an increased susceptibility of Antarctic ice shelves to swell impacts if they continue to thin and be increasingly exposed to low sea ice conditions.

https://doi.org/10.5194/egusphere-2026-3544
Preprint. Discussion started: 9 July 2026

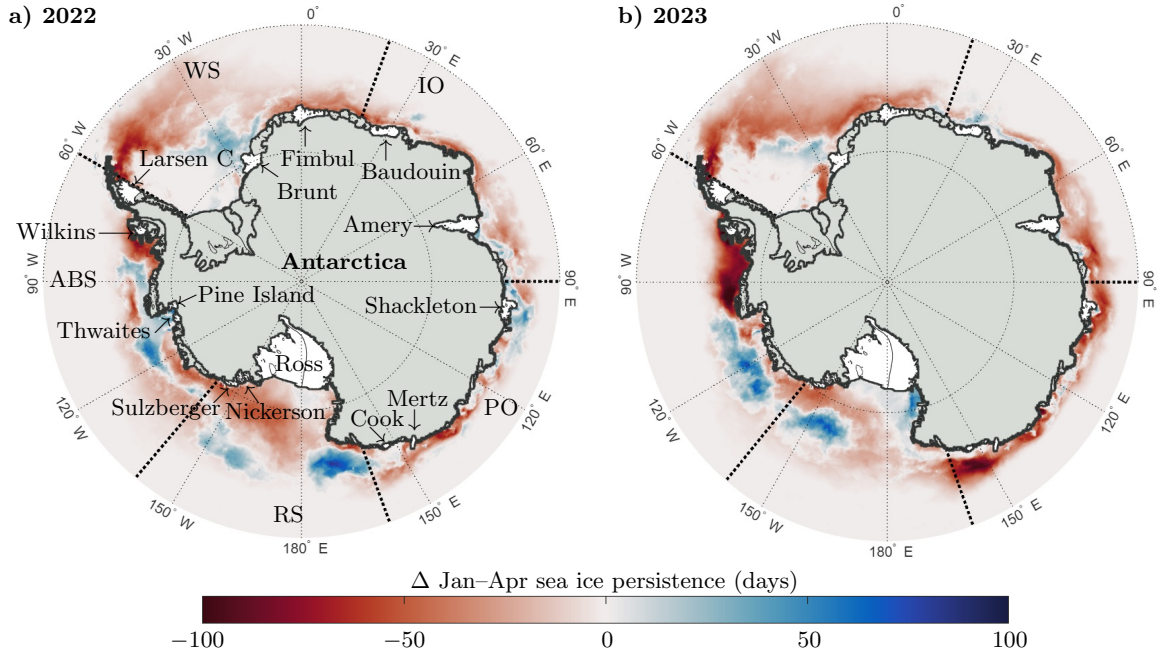

Figure 1. a,b) Map of Antarctica and surrounding ocean showing the change in the number of days where sea ice is present ($\geq$ 15% sea ice concentration) over January–April, for a) 2022 and b) 2023 against the 2014–2021 mean. Overlain are locations and labels for the sea ice sectors used in this study (cf. Zwally, 2002), representing the Weddell Sea (WS; 60°W-20°E), Indian Ocean (IO; 20°E-90°E), Pacific Ocean (PO); 90°E-160°E), Ross Sea (RS; 160°W-140°W) and Amundsen–Bellingshausen Sea (ABS; 140°W-60°E).

2 Methods

2.1 Choice of ice shelves

Fourteen Antarctic ice shelves are considered (Fig. 1a), such that the study encompasses a wide range of ice shelf and sea ice conditions, as well as locations around Antarctica, with each of the Weddell Sea (WS), Indian Ocean (IO), Pacific Ocean (PO), Ross Sea (RS) and Amundsen–Bellingshausen Sea (ABS) sectors represented (Table 1). The 14 ice shelves cover areas from around 5,000 km^2 (Mertz and Cook) to $>$ 50,000 km^2 (Amery) to $>$ 500,000 km^2 (Ross), and they collectively make up $\approx$ 50% of the total ice shelf area around Antarctica (based on 2021 data; Greene et al., 2022). The spatial mean ice shelf thickness ranges from $\approx$ 103 m (Wilkins) to $\approx$ 617 m (Amery), with the mean thickness over all 14 ice shelves $\approx$ 371 m (based on Bedmap2 data; Fretwell et al., 2013). Ice shelves on the East Antarctic Ice Sheet (EAIS) typically extend farther north than

https://doi.org/10.5194/egusphere-2026-3544
Preprint. Discussion started: 9 July 2026

ice shelves on the West Antarctic Ice Sheet (WAIS). Thus, ice shelves on the EAIS (Fimbul, IO, and PO) typically have shorter sea-ice barriers (the length of the region in front of the ice shelf covered in sea ice) than ice shelves on the WAIS, which is quantified in terms of the number of days that effective sea-ice lengths (sea ice length corrected for sea ice concentration; see § 2.2.2) are < 100 km over January–April (the season in which swell typically reaches ice shelves; Teder et al., 2022). Cook on the EAIS (PO) is an exception, as its location traps sea ice, resulting in a small number of short sea-ice barrier days.

The 14 ice shelves are also chosen to include several ice shelves that experienced notable calving events during the study period (2014–2023). A tabular iceberg of $\approx 6000\,km^2$ area calved from Larsen C in 2017 (the A68; Hogg and Gudmundsson, 2017). Brunt experienced multiple tabular calving events from 2021–2024, including the loss of $\approx 1270\,km^2$ of its area in February 2021 (Francis et al., 2022) and $\approx 1550\,km^2$ in 2023 (Marsh et al., 2024). A $106\,km^2$ iceberg calved from Sulzberger in 2022, which was linked with the arrival of a tsunami caused by the Hunga-Tonga volcano eruption (Zhao et al., 2024). Although Shackleton did not experience any major calving events over the study period, the nearby (≈ 60 km east) Conger–Glenzer disintegrated in early 2022, losing 93% of its pre-2020 area (Walker et al., 2024).

Name	**Sector** (Longitude)	**Northern extent**	**Area**	**Thickness**	**Sea-ice barrier**
Larsen C	WS (63.5°W)	66.2°S	Medium	Intermediate	Strong
Brunt	WS (22.5°W)	74.0°S	Medium	Thin	Average
Fimbul	WS (1.5°E)	69.9°S	Medium	Intermediate	Weak
Baudouin	IO (28.4°E)	69.1°S	Medium	Thin	Weak
Amery	IO (70.4°E)	68.6°S	Large	Thick	Average
Shackleton	PO (97.9°E)	65.7°S	Medium	Thin	Weak
Mertz	PO (145.2°E)	66.8°S	Small	Thick	Average
Cook	PO (152.8°E)	68.3°S	Small	Thick	Strong
Ross	RS (175.8°W)	78.0°S	Large	Thick	Average
Nickerson	RS (145.8°W)	75.4°S	Small	Thin	Average
Sulzberger	RS (148.9°W)	76.4°S	Medium	Intermediate	Average
Thwaites	ABS (106.1°W)	74.8°S	Small	Intermediate	Strong
Pine Island	ABS (100.7°W)	74.4°S	Small	Thick	Strong
Wilkins	ABS (71.7°W)	69.7°S	Medium	Thin	Average

Table 1. Relevant ice shelf statistics for each of the 14 ice shelves studied alongside the surrounding sea ice, where the ice shelves are ordered from the East Antarctic Peninsula to West Antarctic Peninsula, starting in the Weddell Sea. Ice shelf area is based on 2021 data (Greene et al., 2022). They are used to classify the ice shelves as large ($> 50{,}000\,km^2$), medium ($10{,}000$–$50{,}000\,km^2$) and small ($< 10{,}000\,km^2$). Ice shelf thickness is based on Bedmap2 data (Fretwell et al., 2013). The spatial mean thickness of an ice shelf is used to classify it as thin (< 300 m), intermediate (300–400 m) or thick (> 400 m). The sea-ice barrier for each ice shelf is classified as strong, average or weak, according to whether the mean number of days per year that its effective sea-ice length (in January–April over 2014–2021; see § 2.2.2) is < 100 km for < 30 days (strong), 30–70 days (average) or > 70 days (weak).

https://doi.org/10.5194/egusphere-2026-3544
Preprint. Discussion started: 9 July 2026

2.2 Data and algorithms

2.2.1 Shelf front thickness

Surface elevation data from Cryosat-2 Synthetic Aperture Radar Interferometry (SARin) Level-2I processing baseline-E mode are used to calculate the ice shelf thickness. The Cryosat-2 satellite was launched on 8 April 2010 and provides coverage to 88° S on a 369-day repeat cycle, and an approximately 30-day sub-cycle. For each of the 14 ice shelves, the following algorithm is used to create a dataset of the ice shelf thickness close to the shelf front, at a 3 km^2 resolution and a yearly frequency over the study period (2014–2023). For ice shelf X in year yyyy:

1. A 3 km^2 grid is calculated with the ice shelf coordinates imported from its boundary in the Making Earth System Data Records for Use in Research Environments (MEaSUREs) Antarctic Boundaries for International Polar Years 2007–2009 from Satellite Radar, Version 2 dataset (Mouginot et al., 2017). A 10 km buffer north of the ice shelf is added to account for potential growth of the ice shelf over the 10-year study period.

2. The shortest distance from each cell within the ice shelf to its front is calculated, with the ice shelf front being defined as cells within < 50 km to the ocean.

3. Elevations with an accompanying ≥ 30 dB of backscatter are removed (Siegfried et al., 2014). Outlier freeboard elevations (e) are also removed to eliminate elevation tracks on the ice sheet. They are determined as $e \notin (e_{25} - 1.5 \times IQR,\ e_{75} + 1.5 \times IQR)$, where e_{25} and e_{75} are the 25th and 75th percentiles of freeboard elevation, and $IQR = e_{75} - e_{25}$ is the interquantile range.

4. Surface freeboard elevations are corrected for tides via the Circum-Antarctic Tidal Simulation (Padman et al., 2002), with ocean-tide loading from the Finite Element Solutions 2004 (FES2004) tidal atlas (Lyard et al., 2006). A dynamic atmospheric correction is applied from Mog2D (Carrère and Lyard, 2003) and the location of the geoid from the Earth Gravitational Models 1996 (EGM1996).

5. Following Chuter and Bamber (2015), the corrected freeboard elevation is converted to ice shelf thickness via

$$h_{\text{sh}} = \frac{(e - \delta)\rho_w}{\rho_w - \rho_i} + \delta, \tag{1}$$

where h_{sh} is ice shelf thickness, δ is the firn air content (Ligtenberg et al., 2014), $\rho_w = 1028\,\text{kg m}^{-3}$ is water density and $\rho_i = 917\,\text{kg m}^{-3}$ is ice shelf density.

6. The 30th percentile of ice shelf thickness values across the retained grid cells is used to represent the thickness $h_{\text{sh}}^{\text{X:yyyy}}$ of ice shelf X in year yyyy.

The 30th percentile is chosen somewhat arbitrarily but noting that thinner sections of the shelf fronts will experience the greatest flexure in response to swell forcing (Liang et al., 2024).

https://doi.org/10.5194/egusphere-2026-3544
Preprint. Discussion started: 9 July 2026

2.2.2 Effective sea-ice length

Sea ice concentration data from the Advanced Microwave Scanning Radiometer (ASMR2) Artist Sea Ice (ASI) dataset are used to calculate the lengths of sea ice cover surrounding the ice shelves. ASMR2 ASI data are available at a daily frequency from July 2012. The AMSR2 ASI dataset uses a 89 GHz channel to produce sea ice concentration, which gives a finer spatial resolution (3.125 km^2) than other sea ice datasets, although it is more susceptible than lower-frequency channels to uncertainties at low sea ice concentrations near the ice edge (Meier et al., 2017). To delineate locations of the ice shelf edge, the no land mask version of the AMSR2 ASI dataset is used, with a coastline mask created by converting the 2013 coastline boundary from Greene et al. (2022) to a 3.125 km^2 grid. The mask flags the cells on the continent edge from which individual ice shelves can be extracted via coordinates from the MEaSUREs dataset.

For each of the 14 ice shelves, the following algorithm (which is similar to that used for the Wilkins and Voyeykov ice shelves over 2002–2009 by Teder et al., 2025) is used to create an "effective" sea-ice-length dataset at a daily frequency from January–April in each of the ten years of the record. For ice shelf X on day ddd of year yyyy:

(a) Straight line "transects" on a polar stereographic projection are calculated between each pair of cells, such that one of the cells is along the shelf front and the other cell is 10° north of the mean shelf front latitude, and ± 45° east of the mean shelf front longitude. The increase to ± 45° (in contrast to Teder et al., 2025) facilitates analysis in the Weddell Sea, due to the dimensions of the embayment. Transects are discarded if they intersect any islands, or any other parts of the coastline. This step generates 20,000–200,000 transects, depending on ice shelf geometry.

(b) For each transect, t, the sea-ice length, $L^{(t)}$, is the aggregate of the lengths of each cell along the transect with a sea ice concentration $> 15\%$, and the concentration, $C^{(t)}$, is the average sea ice concentration of these cells.

(c) Effective sea-ice lengths for each transect are calculated as

$$L_{\text{eff}}^{(t)} = L^{(t)}\, C^{(t)}. \tag{2}$$

(d) The 10th percentile of the effective sea-ice lengths over all transects are used as the effective sea-ice length $L_{\text{eff}}^{\text{X:ddd-yyyy}}$ for the sea-ice barrier surrounding ice shelf X on day ddd in year yyyy.

The 10th percentile was chosen to represent vulnerable sections of the sea-ice barrier, through which incoming swell will most readily reach a shelf front.

2.2.3 Incoming swell

Swell properties are extracted from the Collaboration for Australian Weather and Climate Research (CAWCR) Wave Hindcast - Aggregate Collection (Smith et al., 2020). The CAWCR hindcast starts on 1 January 1979, and provides hourly outputs

https://doi.org/10.5194/egusphere-2026-3544
Preprint. Discussion started: 9 July 2026

on a 0.4° spatial grid of the ocean surface, where the operational range extends to 78° S. It is generated using the WaveWatch III v4.18 wave model and forced with hourly 10 m surface winds and daily sea ice concentration data from the National Center for Atmospheric Research Climate Forecasts System Version 2 reanalysis (since 2011). Swell data are used up to sea-ice concentrations of 25%, for which the hindcast is considered unaffected by the presence of sea ice (Tolman, 2003).

For each of the 14 ice shelves, the following algorithm is used to calculate datasets of incoming swell, in terms of significant wave height and peak period, at a daily frequency over January–April in each of the ten years of the record. For ice shelf X on day ddd of year yyyy:

1. Calculate the ocean cells (sea ice concentrations $< 25\%$) along the straight-line transects.
2. For each hour during the day (h), take the maximum values of significant wave height and peak period over the ocean cells, $H_{\mathrm{s}}^{\mathrm{h,max}}$ and $T_{\mathrm{p}}^{\mathrm{h,max}}$, respectively.
3. The 90th percentiles of the maximum hourly values are used for the daily significant wave height and peak period, $H_{\mathrm{s}}^{\mathrm{X:ddd\text{-}yyyy}}$ and $T_{\mathrm{p}}^{\mathrm{X:ddd\text{-}yyyy}}$.

The maximum hourly values of significant wave height and peak period (Step 2) and the 90th percentiles of the hourly values (Step 3) are chosen in to capture the potentially most damaging swell in the relevant region.

2.3 Swell–sea ice–ice shelf model

A modified version of the Teder et al. (2025) model is used to predict the flexural stress imposed by incoming swell on an ice shelf after it has been attenuated by the sea-ice barrier protecting the ice shelf (Fig. 2a). The overall swell–sea ice–ice shelf model combines a model of swell attenuation over distance through a region of sea ice cover (Fig. 2b) and a model swell-induced flexure of an ice shelf (Fig. 2c).

https://doi.org/10.5194/egusphere-2026-3544
Preprint. Discussion started: 9 July 2026

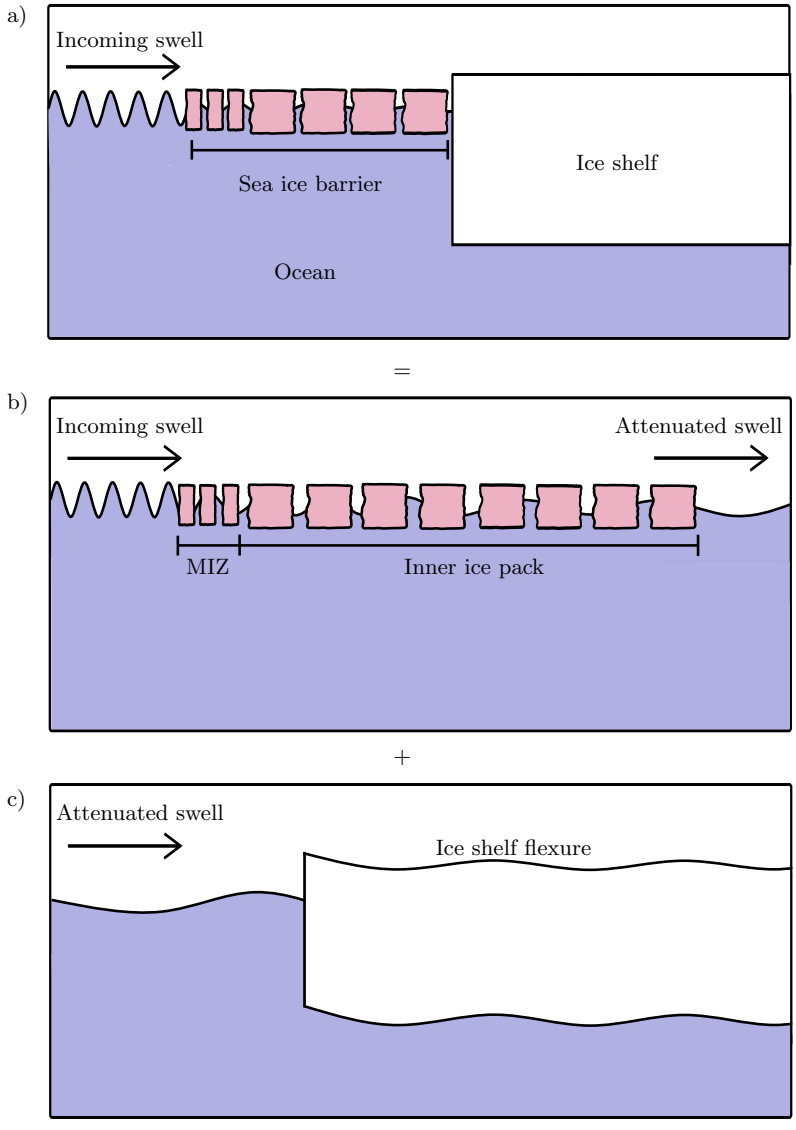

Figure 2. a) Model schematic, indicating incoming swell from the open ocean being attenuated by sea ice before reaching an ice shelf and forcing the ice shelf to flex (§ 2.3.3). The full model combines two sub-models: b) swell attenuation over distance through a sea ice cover, where the sea ice cover consists of a marginal ice zone and an inner ice pack (§ 2.3.1); and c) swell-induced flexure of an ice shelf (§ 2.3.2).

https://doi.org/10.5194/egusphere-2026-3544
Preprint. Discussion started: 9 July 2026

2.3.1 Swell attenuation by sea ice

A two-dimensional model is used to predict the attenuation of swell over distance travelled through the sea ice covered ocean, involving one horizontal dimension in the direction of swell propagation, and one depth dimension. The ice cover is treated as a collection of ice floes, which are modelled as Kirchoff plates with Young's modulus $E = 6\,\text{GPa}$ (Williams et al., 2013a), floating on an ocean modelled as an inviscid and incompressible water domain that undergoes irrotational motions. As standard, the vertical amplitudes of motion are considered small relative to the wavelengths involved, such that the model may be linearised and decomposed into its different wave period components, i.e., its regular wave components (Squire, 2020; Golden et al., 2020; Bennetts, 2025).

Consistent with observations, models of this form typically predict exponential attenuation rates (Bennetts, 2025), such that

$$A_L \approx A_0 \exp(-\alpha\, x) \tag{3}$$

where A_L is the swell amplitude at propagation distance L, A_0 is the initial amplitude, and α is the attenuation coefficient (i.e., the exponential rate of attenuation), which is a function of wave period, T. The attenuation coefficient is partitioned as $\alpha = \alpha_{\text{sca}} + \alpha_{\text{dis}}$, where α_{sca} is attenuation due to wave scattering and α_{dis} is attenuation due to dissipative processes. Assuming random wave phases, attenuation due to scattering is approximated following Bennetts and Squire (2012b)

$$\alpha_{\text{sca}} = -\frac{C \ln(1-\mathcal{R}^2)}{d}, \tag{4}$$

where C is the sea ice concentration, d is the floe size, and $\mathcal{R} \approx \tanh(a_0 + a_1\, h_{\text{fl}})$ is the proportion of an incident wave amplitude reflected by an floe edge of thickness h_{fl}, where a_0 and a_1 depend on wave period (Bennetts and Squire, 2012a). Attenuation due to dissipation is modelled as drag pressure at the ocean–floe interface, using the so-called Robinson–Palmer model with a drag parameter of $13.5\,\text{Pa s m}^{-1}$ and scaled by the sea ice concentration, which is also a function of wave period (Williams et al., 2013a, b; Massom et al., 2018).

The e-fold attenuation distance (α^{-1}) is a measure of how far swell is able to travel through the sea ice covered ocean (Fig. 3). It increases greatly as wave period increases over the swell regime, going from $< 25\,\text{km}$ at $T = 8\,\text{s}$ to $> 200\,\text{km}$ at $T = 20\,\text{s}$. It also increases with increasing floe size, but with notable changes occurring only for floe sizes approximately $< 250\,\text{m}$ and with a weakening influence as wave period increases.

https://doi.org/10.5194/egusphere-2026-3544
Preprint. Discussion started: 9 July 2026

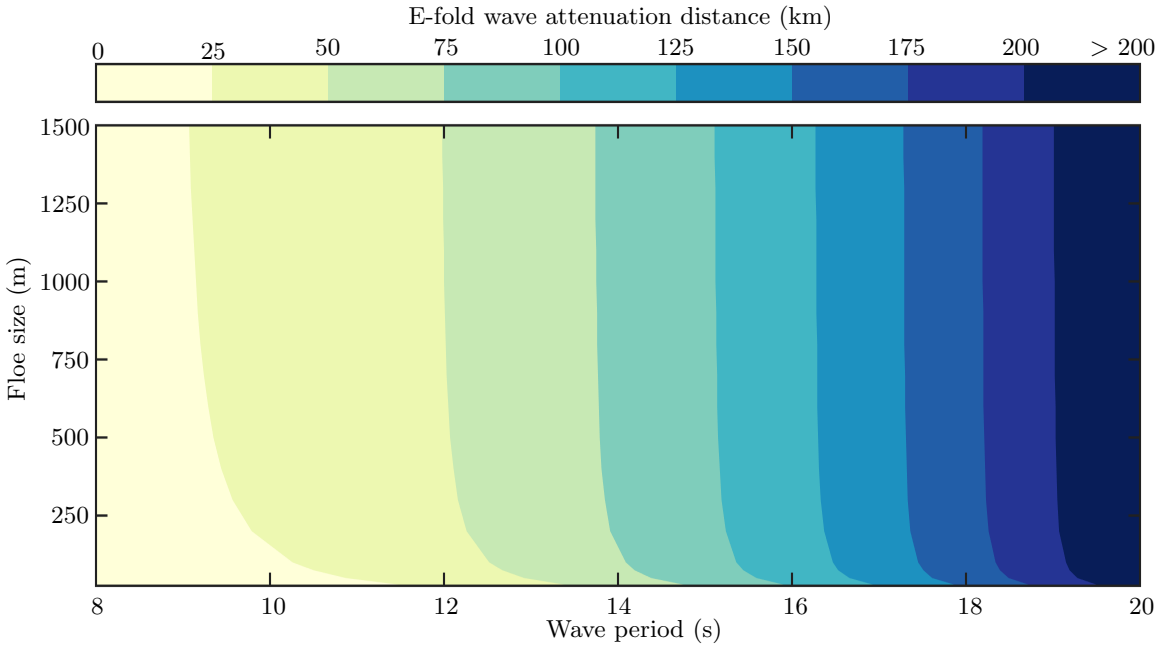

Figure 3. Swell attenuation by sea ice model (§ 2.3.1) predictions of e-fold attenuation distance (α^{-1}) vs. wave period and floe size.

2.3.2 Ice shelf flexural stress

A different model is used to predict the flexural stress experienced by an ice shelf in response to swell forcing (Bennetts, 2025). The ice shelf is modelled as a floating Kirchoff plate of semi-infinite length, with thickness h_{sh}, Poisson's ratio $\nu = 0.3$, and Young's modulus $E = 9\,\text{GPa}$ (Liang et al., 2024). Adopting similar assumptions to the model of swell attenuation in the sea ice covered ocean (§ 2.3.1), the model is used to predict the ice shelf flexural displacement, $\eta(x)$, where x is the distance from the ice edge, in response to a regular incoming wave of amplitude, A, and prescribed wave period, T (Bennetts et al., 2022). Due to linearity, the ice shelf flexural displacement is

$$\eta(x) = A\,\hat{\eta}(x), \tag{5}$$

where $\hat{\eta}$ is the flexural displacement in response to unit-amplitude forcing. The flexural stress is then

$$\sigma = \frac{E\,h}{2\,(1-\nu^2)}\,\eta'', \tag{6}$$

where primes denote differentiation with respect to x.

The spatial maximum flexural stress due to swell forcing, $\max_x |\sigma|$ (which occurs in the shelf front region; Massom et al., 2018), increases with wave period and decreases with ice shelf thickness (Fig. 4). For swell forcing with amplitude $A = 1\,\text{m}$,

https://doi.org/10.5194/egusphere-2026-3544
Preprint. Discussion started: 9 July 2026

the stress reaches potentially significant levels of > 10 kPa (Bassis et al., 2024) within the swell regime ($T = 8$–20 s) for ice shelves thinner than ≈ 240 m. At an ice shelf thickness of ≈ 110 m, σ is > 10 kPa for over half of the wave period range ($T = 14$–20 s). For very thin ice shelves (approximately < 100 m), flexural stress can reach values > 100 kPa.

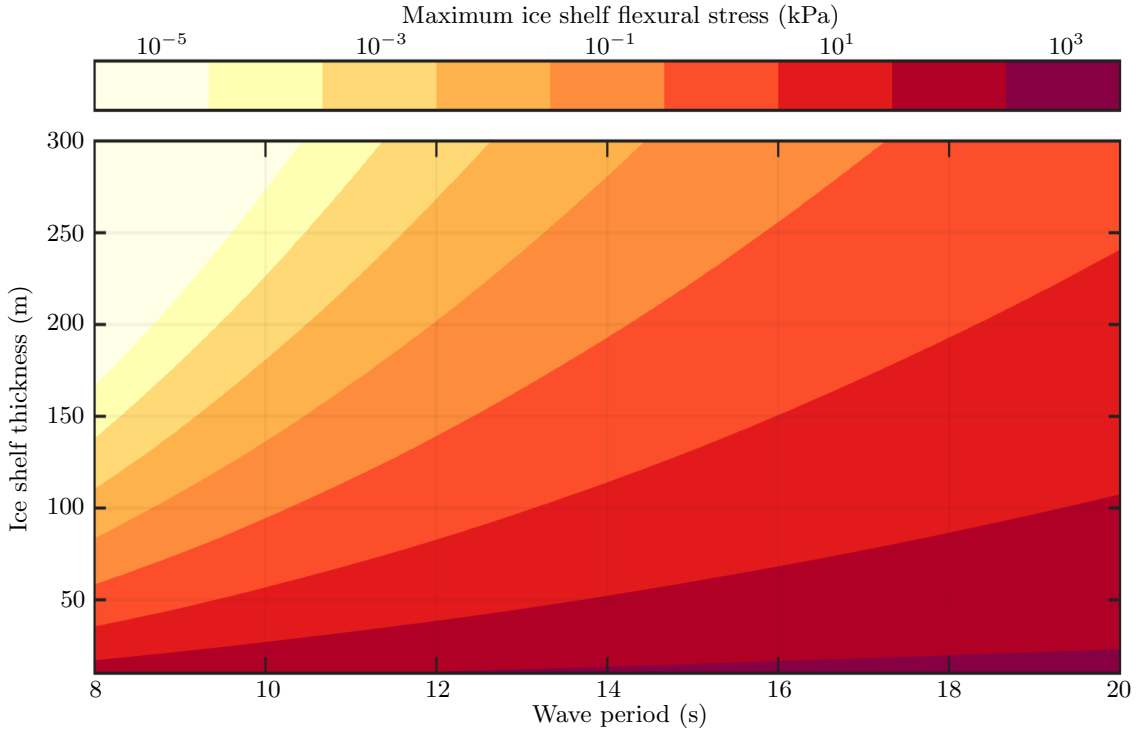

Figure 4. Ice shelf flexural stress model (§ 2.3.2) predictions of maximum stress ($\max_x |\sigma|$) created by a swell of amplitude $A = 1$ m vs. wave period and ice shelf thickness.

2.3.3 Combined model and outputs

190 The above models (§ 2.3.1–§ 2.3.2) are combined to predict the flexural stress, $\sigma^{\text{X:ddd–yyyy}}$, experienced by ice shelf X on day ddd of year yyyy, in response to incoming swell from the sea-ice free ocean, after the swell has been attenuated by the surrounding sea ice cover (Fig. 2a-c). The ice shelf thickness is set as $h_{\text{sh}} = h_{\text{sh}}^{\text{X:yyyy}}$, the sea-ice length as $L = L_{\text{eff}}^{\text{X:ddd–yyyy}}$ (i.e., 100% sea ice concentration is used in the model), and the incoming swell amplitude and wave period as $A_{\text{inc}} = 0.5\, H_{\text{s}}^{\text{X:ddd–yyyy}}$ and $T = T_{\text{p}}^{\text{X:ddd–yyyy}}$.

https://doi.org/10.5194/egusphere-2026-3544
Preprint. Discussion started: 9 July 2026

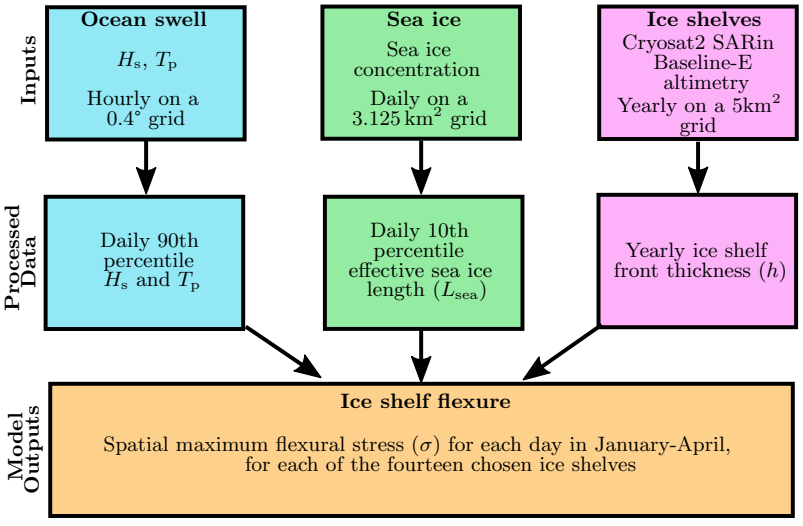

Figure 5. Workflow of the swell–sea ice-ice-shelf model (§ 2.3.3), as applied for each of the fourteen ice shelves considered in this study, for each day in January–April over 2014–2023.

The sea ice cover is divided into the marginal ice zone (MIZ), which is taken to occupy the first 15% of the effective sea-ice length from the sea-ice free ocean (Fraser et al., 2026), and the inner ice pack zone that occupies the remaining 85%. In the MIZ, the ice floe thickness and size are set as $h_{\rm fl} = 0.27\,$m and $d_{\rm fl} = 37\,$m, respectively, and in the inner ice pack they are $h_{\rm fl} = 1.4\,$m thick and $d_{\rm fl} = 800\,$m (Kurtz and Markus, 2012; Day et al., 2024). Thus, the amplitude of swell reaching the shelf front is

$$A_{\rm atn} = A_{\rm inc} \exp\{-(0.15\,\alpha_{\rm miz} + 0.85\,\alpha_{\rm pac})\,L\}, \tag{7}$$

where $\alpha_{\rm miz}$ and $\alpha_{\rm pac}$, respectively, denote the attenuation coefficients for the MIZ and inner ice pack, using the prescribed floe thickness and size for the two regions. The ice shelf flexural displacement is $\eta = A_{\rm atn}\,\hat{\eta}$ and the corresponding flexural stress is calculated via (6). For each of the 14 ice shelves (X), the combined model is used to generate daily (ddd) records over the yyyy =2014–2023 study period of the flexural stress, $\sigma^{\rm X:ddd–yyyy}$ (Fig. 5).

https://doi.org/10.5194/egusphere-2026-3544
Preprint. Discussion started: 9 July 2026

3 Results

3.1 Changes in individual drivers

3.1.1 Changes in shelf front thickness

Baseline values of mean shelf front thicknesses ($h_{\mathrm{sh}}^{\mathrm{X:yyyy}}$; § 2.2.1) are calculated for each ice shelf over the years 2014–2021 (i.e., prior to the extreme sea-ice lows of 2022 and 2023; Fig 6a). The baseline shelf front thickness values range from 56 m for Wilkins and 130 m for Brunt, to 312 m for Amery and 338 m for Ross. The mean thickness over the 14 ice shelves is 225 m, with a standard deviation of 77 m.

Six of the 14 ice shelves are thinner in both 2022 and 2023 than the 2014–2021 baseline (Mertz, Cook, Thwaites, Pine Island, Wilkins, Brunt; Fig. 6b). The largest proportional reductions are for Mertz ($>$ 6% in 2022 and 2023), Cook ($\approx$ 5% in 2022) and Pine Island ($>$ 7% in 2022 and $\approx$ 5% in 2023). Thinning of the Brunt and Cook shelf fronts contrast with their 1997–2021 thickening trends (Davison et al., 2023). The Cook shelf front thinned as it expanded northwards (Greene et al., 2022), whereas the Brunt shelf front calved in 2021 and 2023, removing thicker portions of the shelf front (Marsh et al., 2024).

Five of the 14 shelf fronts were thicker in both 2022 and 2023 compared to their respective 2014–2021 baseline thickness values (Baudouin, Shackleton, Ross, Nickerson, Larsen C). The proportional thickness increases for these five ice shelves are generally less than the decreases experienced by the six ice shelves noted above. The greatest thickness increases are for Shackleton ($\approx$ 3% in 2023), Nickerson ($\approx$ 2.5% in 2023) and Larsen C ($\approx$ 3% in 2022 and 2% in 2023).

The remaining three ice shelves (Fimbul, Amery, Shackleton) experienced one year of increased and one of decreased thickness. The absolute changes for Fimbul and Amery are $<$1% only. In contrast, Sulzberger thinned by $\approx$ 2.5% in 2022 before thickening by $\approx$ 4% in 2023, where the latter is likely a result of its calving in 2022 (Zhao et al., 2024).

https://doi.org/10.5194/egusphere-2026-3544
Preprint. Discussion started: 9 July 2026

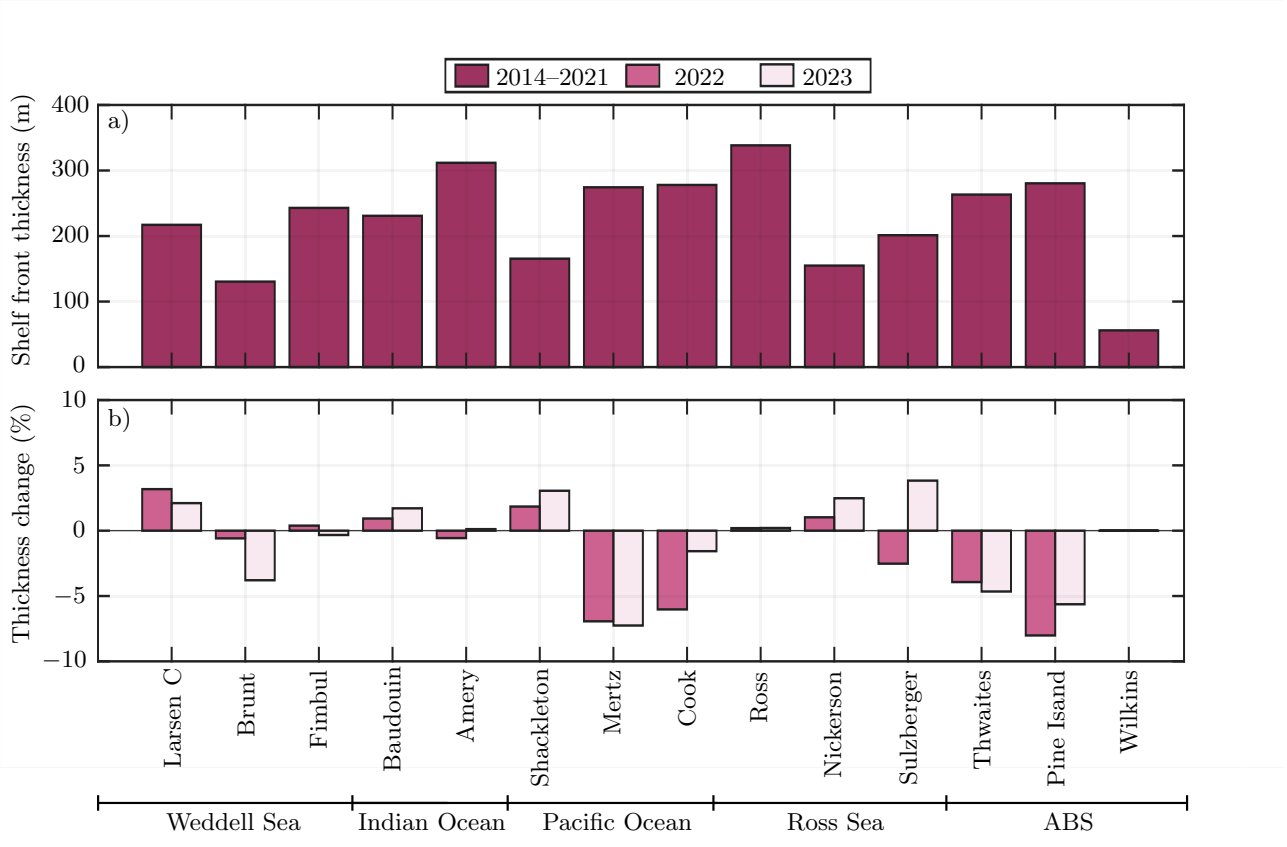

Figure 6. a) Mean shelf front thickness for each shelf over 2014–2021 (dark maroon). b) Percentage change in shelf front thickness for each ice shelf in 2022 (light maroon) and 2023 (off-white), compared to their corresponding 2014–2021 values. (Nb. A technical problem with Cryosat-2 necessitated use of the 2022 Wilkins shelf front thickness for its 2023 thickness.)

https://doi.org/10.5194/egusphere-2026-3544
Preprint. Discussion started: 9 July 2026

3.1.2 Changes in effective sea-ice length

Baseline datasets for effective sea-ice length ($L_{\mathrm{eff}}^{\mathrm{X:ddd-yyyy}}$; § 2.2.2) prior to the sea ice lows of 2022–2023 are calculated for each ice shelf over days in January–April and years 2014–2021 (Fig. 7). The median baseline effective sea-ice length spans 43.90 km for Shackleton to 507.90 km for Larsen C, and the median effecive sea-ice length over all 14 ice shelves is 55.67 km. The interquartile ranges span 40.06 km for Fimbul to 662.16 km for Ross.

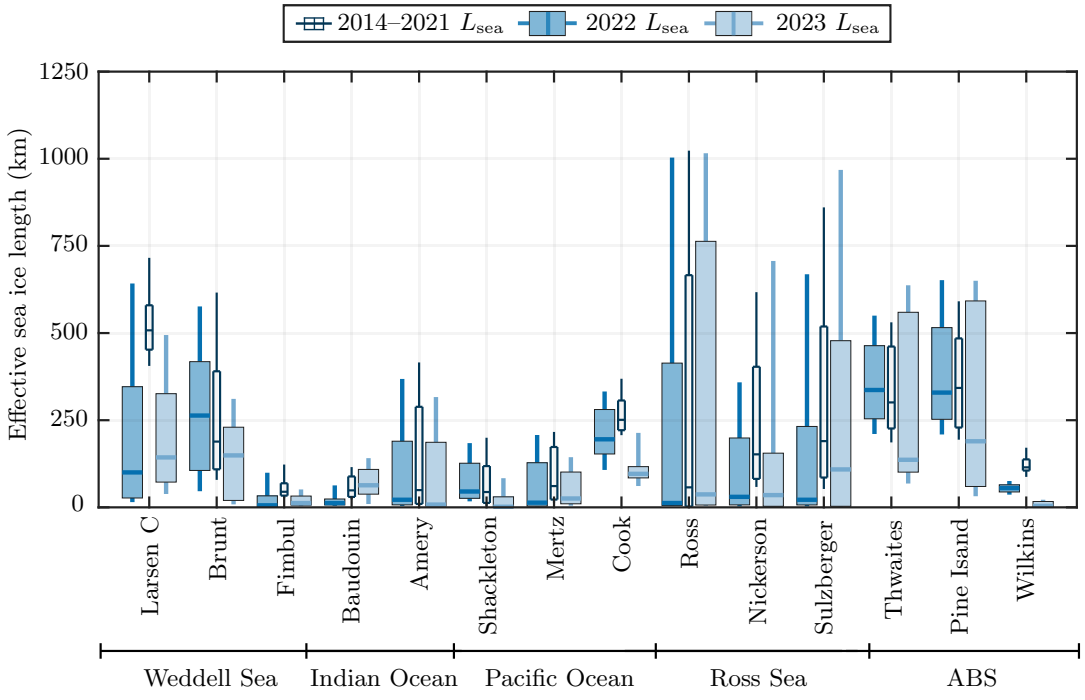

Figure 7. Statistics of effective sea-ice length for each ice shelf during January–April, in terms of interquartile ranges (boxes), median values (horizontal lines within boxes), and minimum and maximum values (vertical lines). Results are for 2022 (blue), 2023 (light blue), and 2014–2021 (thin white boxes).

The median effective sea-ice length over all 14 ice shelves drops to 37.79 km in 2022, but is 50.23 km in 2023, i.e., only slightly below the baseline value. Although the median effective sea-ice length is greater in 2023 than 2022, the 25th and 75th percentiles tend to be smaller in 2023, which indicates the low sea ice conditions persist for longer periods during January-April in 2023.

https://doi.org/10.5194/egusphere-2026-3544
Preprint. Discussion started: 9 July 2026

In 2022–2023 combined, there are 24 instances of reduced median sea-ice length in comparison to the baseline values, with an average decrease of 46.10% ± 42.40% in 2022 and 56.20% ± 33.30 in 2023. Ice shelves in the Weddell Sea (Larsen C, Fimbul), Indian Ocean (Shackleton, Mertz, Cook), Ross Sea (Ross, Nickerson, Sulzberger) and Amundsen-Bellingshausen Sea (Thwaites, Wilkins) have reduced median effective sea-ice lengths in 2022 and 2023, of which six ice shelves (Larsen C, Fimbul, Amery, Mertz, Nickerson, Wilkins) have >50% decreases in both years. Eight ice shelves have a minimum effective sea-ice length < 10 km in 2022, and ten in 2023, with seven instances < 10 km shared between both years (Baudouin, Amery, Ross, Nickerson, Sulzberger, Fimbul and Mertz). Only three ice shelves (Thwaites, Pine Island, Cook) have a minimum sea-ice length > 10 km in 2022 and 2023.

3.1.3 Changes in incoming swell

Baseline datasets for the peak period of incoming swell ($T_{\mathrm{p}}^{\mathrm{X:ddd\text{-}yyyy}}$; § 2.2.3) are calculated for each ice shelf over days in January–April for years 2014–2021 (Fig. 8). Similar baselines datasets are calculated for significant wave height (Fig. 9). The median baseline peak period and significant wave height span 11.14 s (Brunt) to 14.29 s (Shackleton) and 2.49 m (Ross) to 5.43 m (Shackleton), respectively. The medians over the 14 ice shelves are 12.99 s for peak period and 4.14 m for significant wave height. Ice shelves in the Indian and Pacific Oceans have the largest peak periods (median 13.33 s) and significant wave heights (median 5.08 m), which is consistent with satellite observations of the greatest Southern Ocean wave heights being in the 60-120°E sector (Young et al., 2020).

https://doi.org/10.5194/egusphere-2026-3544
Preprint. Discussion started: 9 July 2026

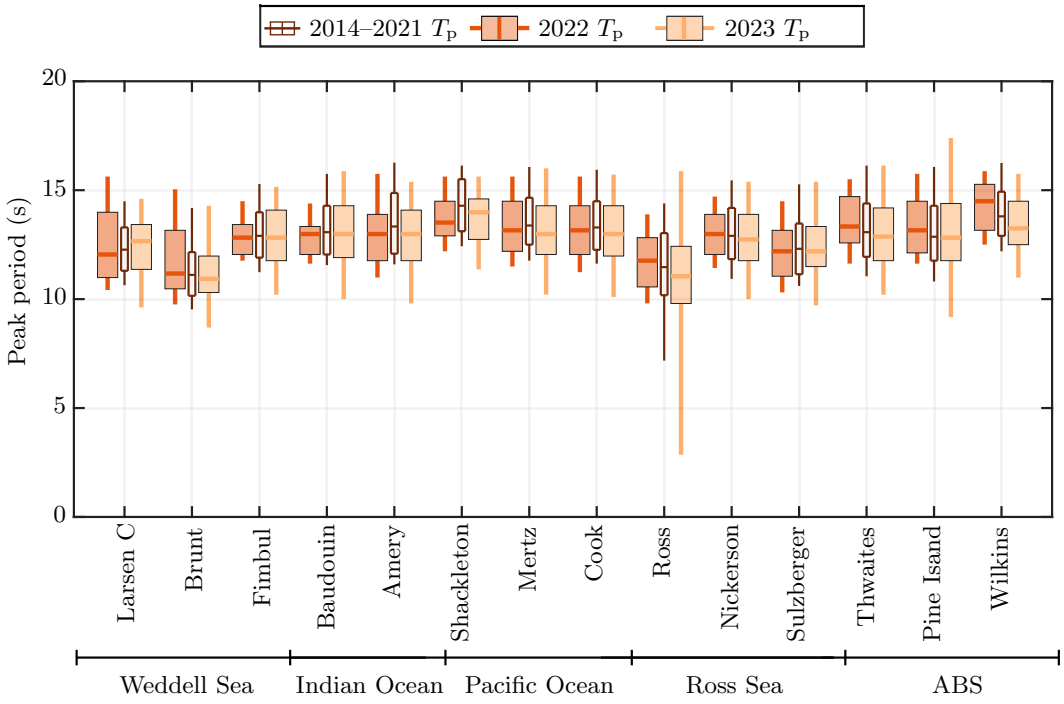

Figure 8. As in Fig. 7, but for peak period of incoming swell.

The median peak period and significant wave height over all 14 ice shelves are 12.98 s and 4.56 m in 2022, and 12.85 s and 4.04 m in 2023. Relative to the corresponding baseline values, these are decreases in peak period of 0.07% and 1.08% in 2022 and 2023, respectively, alongisde a significant wave height increase of 3.11% in 2022 and decrease of 2.27% in 2023. In 2022, the median values for peak period and significant wave height increased for six ice shelves on the WAIS (Ross, Nickerson, Thwaites, Pine Island, Wilkins, Brunt), and decreased for four ice shelves (Larsen C, Amery, Shackleton, Sulzberger). In 2023, the median values for peak period and significant wave height increased only for the Larsen C and decreased for ten ice shelves (Shackleton, Mertz, Cook, Ross, Nickerson, Sulzberger, Thwaites, Pine Island, Fimbul, Baudouin), covering all five sectors. The 25th percentiles also decrease in 2023, by 1.34% for peak period and 1.00% significant wave height. The decreases are likely linked to a weakening in Southern Ocean wave power in the late 2010s–early 2020s compared to the mid-2010s (Liu et al., 2024).

https://doi.org/10.5194/egusphere-2026-3544
Preprint. Discussion started: 9 July 2026

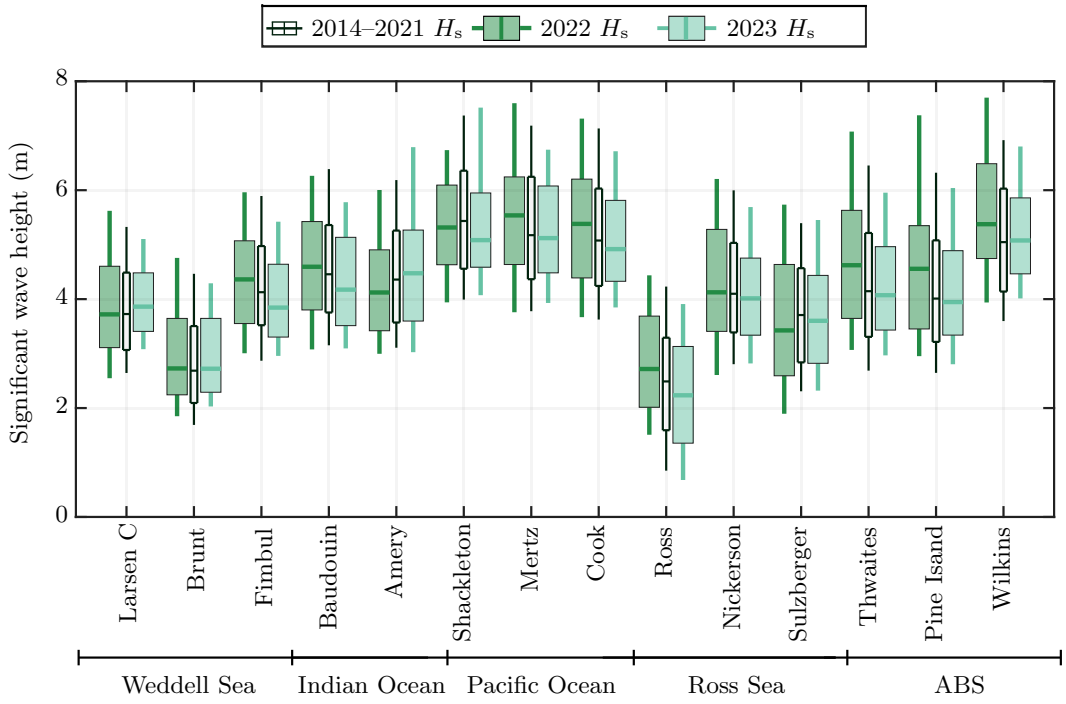

Figure 9. As in Figs. 7–8, but for significant wave height of incoming swell.

3.2 Changes in ice-shelf front flexural stress

The combined model (§ 2.3.3) is used to calculate baseline datasets of flexural stress ($\max_x |\sigma^{\text{X:ddd–yyyy}}|$) for each ice shelf over days in January–April and year 2014–2021 calculated from, and expressed in terms of median and 90th percentile values (Table 2). Wilkins has a considerably thinner shelf front than the other ice shelves studied, h_{sh} <60 m, which, combined with its relatively short effective sea-ice length, gives it the greatest baseline flexural stress levels by an order of magnitude, at order 10 kPa for median and order 100 kPa for 90th percentile. The next three thinnest ice shelves (Shackleton, Nickerson, Brunt; $h_{\text{sh}} = 100$–200 m) have close to the next three largest baseline flexural stress levels at the 90th percentile level. Brunt is the thinnest of these three ice shelves but has the lowest baseline flexural stress levels of the three at both median and 90th percentile, as it has the longest effective sea-ice barrier (Figs. 8–9). Its baseline 90th percentile is slightly smaller than that of Baudouin, and its median baseline flexural stress is far below many of the other studied ice shelves. Fimbul, Sulzberger and Baudouin have slightly thicker shelf fronts (h_{sh} =200–250 m), and, generally, slightly lower baseline stress levels. Larsen C has

https://doi.org/10.5194/egusphere-2026-3544
Preprint. Discussion started: 9 July 2026

much lower baseline stress levels (median order $<10^{-3}$ kPa and 90th percentile order 0.1 kPa), in spite of having a comparable shelf front thickness (h_{sh} =217 m), as it has the longest effective sea-ice barrier of all of the ice shelves considered. Ice shelves with thicker shelf fronts (h_{sh} >250 m; Amery, Mertz, Cook, Ross, Thwaites, Pine Island) generally have very low baseline stress levels, of up to order 0.01 kPa for median and 0.1 kPa for 90th percentile. Mertz is the exception, with order 0.1 kPa for median and order 1 kPa for 90th percentile, as it has the shortest effective sea-ice length (Fig. 7) and strongest incoming swell (Figs. 8–9) of the thick ice shelves over 2014–2021.

Name (Sector)	**2014–2021**		**2022**		**2023**	
	Median	90th percentile	Median	90th percentile	Median	90th percentile
Larsen C (WS)	0.000	0.079	0.030	1.910	0.041	0.806
Brunt (WS)	0.020	3.316	0.031	2.756	0.214	3.744
Fimbul (WS)	0.168	2.028	0.316	1.747	0.246	2.978
Baudouin (IO)	0.391	3.760	0.540	2.412	0.204	3.497
Amery (IO)	0.041	0.873	0.016	0.697	0.024	0.729
Shackleton (PO)	5.008	26.336	3.167	13.760	5.544	24.538
Mertz (PO)	0.132	2.042	0.287	1.939	0.306	2.467
Cook (PO)	0.008	0.446	0.027	0.380	0.057	0.961
Ross (RS)	0.001	0.154	0.001	0.065	0.000	0.364
Nickerson (RS)	0.291	8.045	1.690	10.259	1.433	16.948
Sulzberger (RS)	0.013	1.619	0.196	2.660	0.036	1.754
Thwaites (ABS)	0.004	0.637	0.006	0.213	0.016	1.537
Pine Island (ABS)	0.000	0.406	0.003	0.212	0.008	1.580
Wilkins (ABS)	58.094	248.72	185.782	439.87	204.142	562.67

Table 2. Model predictions of median and 90th percentile flexural stress imposed on each ice shelf from daily values over January–April, for 2014–2021, 2022 and 2023. Flexural stress values in 2022 and 2023 are coloured according to the percentage change from the corresponding 2014–2021 values, in 100% bands: −100–0% (teal); 0–100% (gold); 100–200% (orange); 200–300% (red); > 300% (maroon).

Ice shelves in the eastern Weddell Sea (Brunt, Fimbul), Indian Ocean (Baudouin, Amery), Western Pacific Ocean (Shackleton, Cook) and the Ross have slightly lower 90th percentile stress levels in 2022 than their 2014–2021 baselines (reduced by ≈ 50 % at most). The reductions are generally driven by the incoming swell having shorter wave periods (Fig. 8), in some cases exacerbated by smaller significant wave heights (Fig. 9) and/or thicker shelf fronts (Fig. 6b), which outweigh any increases in stress due to the reduction in effective sea-ice length (Fig. 7). However, their median stress levels are split between slight decreases (Amery, Shackleton, Ross) and increases (Brunt, Fimbul, Baudouin, Mertz, Cook), due to variability in the changes of incoming swell and effective sea-ice length around the median values (between the quartiles), noting that the relative daily changes are a factor in these cases (not shown). In contrast, ice shelves in the western Ross Sea (Sulzberger, Nickerson), Amundsen-Bellingshausen seas (Wilkins) and eastern Weddell Sea (Larsen C) have increased stress levels (median and 90th

https://doi.org/10.5194/egusphere-2026-3544
Preprint. Discussion started: 9 July 2026

percentile), which are driven by reduced effective sea-ice length. Larsen C has the greatest increases in stress levels, which are over 300 % for both median and 90th percentile. Thwaites and Pine Island are the exceptions in these sectors, as they have longer effective sea-ice barriers in 2022 compared to 2014–2021 (likely due to shifting of the Amundsen Sea Low; Wang et al., 2023), which act to outweigh their shelf front thinning and increases in peak period and significant wave height.

Overall, stress levels increase by a greater amount in 2023 compared to 2022. In particular, median and 90th percentile stress levels increase in the eastern Weddell Sea (Brunt, Fimbul), and for the eastern Pacific Ocean (Mertz, Cook), as the effective sea-ice length reductions are strong enough to outweigh any reductions in peak period and significant wave height (Figs. 8–9), and increases in shelf front thickness (Fig. 6b). Further, the flexural stress levels of Thwaites and Pine Island increase by 100–300% for 90th percentile and >300% for median, highlighting that their severe thinning (Fig. 6b) alongside a retreating effective sea-ice length made them particularly susceptible to wave period increases (cf. Fig. 4). Decreased stress levels occurred for the Baudouin and Amery at median and 90th percentile and Shackleton at 90th percentile, as they have short baseline effective sea-ice barriers, making them susceptible to weakening of incoming swell.

3.3 Statistical analysis of swell-induced flexural stress anomalies

The 90th percentile flexural stress anomalies (in terms of modified z-scores) for each of the 14 ice shelves in each of the ten years (2014–2023) are shown against corresponding anomalies in effective sea-ice length, peak period, significant wave height and shelf front thickness (Fig. 10). There are statistically significant correlations (p-values ≈ 0) between stress anomalies and anomalies in effective sea-ice length (negative correlation, $\rho < 0$; Fig. 10a) and peak period (positive correlation, $\rho > 0$; Fig. 10b). The correlations between stress anomalies and anomalies in significant wave height and shelf front thickness are relatively weak (absolute ρ-values are an order of magnitude smaller) and the p-values are considerably larger, such that the correlations are not statistically significant (Fig. 10c,d). These relationships are robust when partial correlations (controlling for other variables) are applied, with ρ for ice length and peak period increasing by a factor of $\approx$1.08 and $\approx$1.21 respectively (not shown).

https://doi.org/10.5194/egusphere-2026-3544
Preprint. Discussion started: 9 July 2026

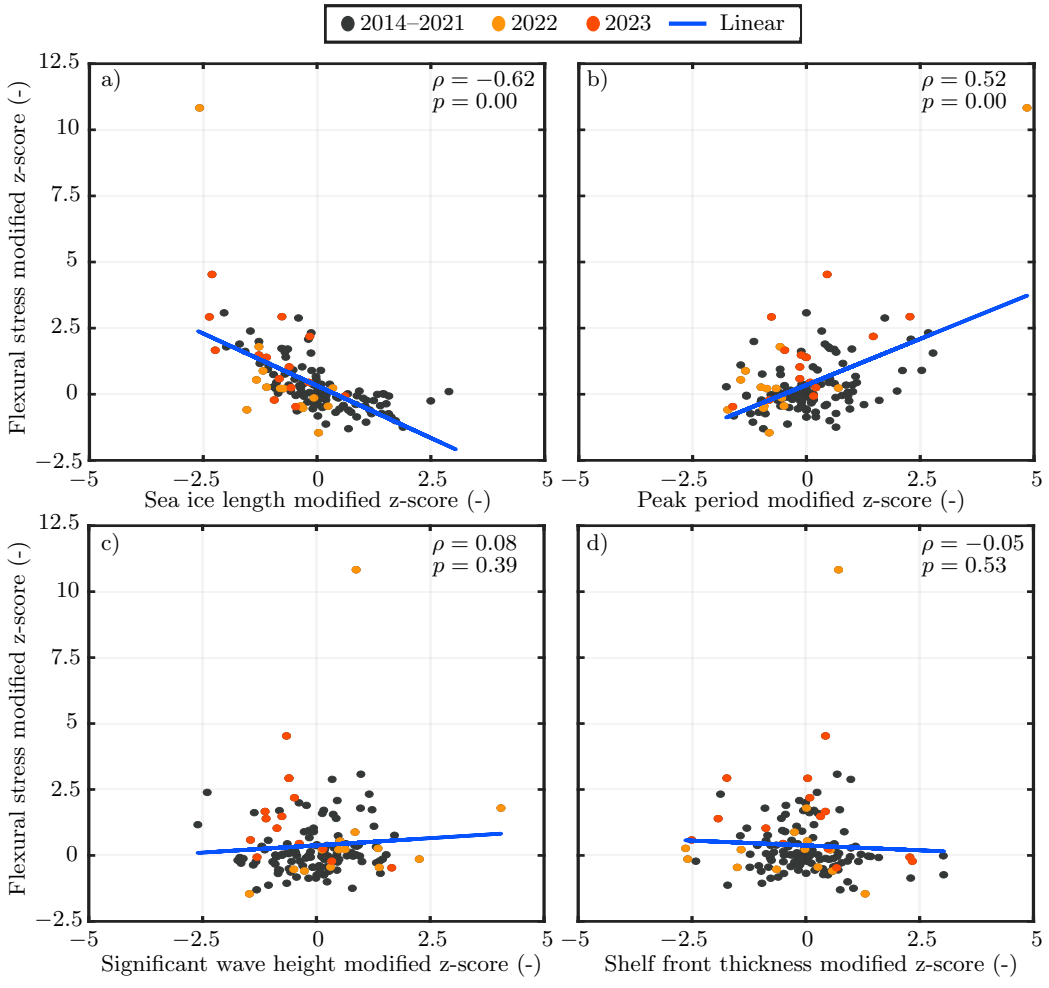

Figure 10. Ninety percentile flexural stress anomalies (z-score) versus anomalies in a) sea-ice lengths, b) peak wave periods, c) significant wave heights, and d) shelf front thickness. A data point is given for each of the 14 ice shelves studied in each year, 2014–2021 (black), 2022 (orange) and 2023 (red). Linear regressions are superimposed (blue lines), along with correlation coefficients (ρ) and p-values (p) from two-sided t-tests.

https://doi.org/10.5194/egusphere-2026-3544
Preprint. Discussion started: 9 July 2026

Based on the statistically significant relationships for flexural stress anomalies with anomalies in effective sea-ice length and peak period, data triplets are created for each shelf in each year (2014–2023) that denote the changes in median values over the year (January–April) for flexural stress, effective sea-ice length and peak period versus the respective median values over the ten years. A support vector machine model is applied to the triplets over 2014–2021 to define a linear boundary in effective sea-ice length–peak period space that separates positive and negative changes in the flexural stress (Fig. 11). The predicted boundary has a positive slope in terms of changes in peak period versus effective sea-ice length, such that smaller reductions in effective sea-ice length (including negative reductions) are required to create increases in flexural stress if peak period increases. The model correctly predicts 15 out of 19 stress increases in 2022–2023 alongside eight out of nine instances of decreased stress. There are five instances of false prediction (either false increases or false decreases), but all lie within the error range. More false predictions occur in 2022 (four) than 2023 (one). All four false predictions in 2022 (Fimbul, Mertz, Nickerson, Sulzberger) are predicted to have reduced stress ($\Delta\sigma < 0$) and are for ice shelves with a median effective sea-ice length < 20 km, such that although the absolute reduction in effective sea-ice length is small, the reduction relative the baseline effective sea-ice length is large, and outweighs the reduction in peak period (Fig. 11a,b). The ice shelf with the false prediction in 2023 (Baudouin) also has reduced stress, in this case caused by a decrease in significant wave height (Fig. 9) and increased thickness (Fig. 6b), which are not considered in the support vector machine model. The moderately strong predictive capabilities of the model are backed by Matthews correlation coefficients of 0.69, alongside an area under curve of 0.90.

https://doi.org/10.5194/egusphere-2026-3544
Preprint. Discussion started: 9 July 2026

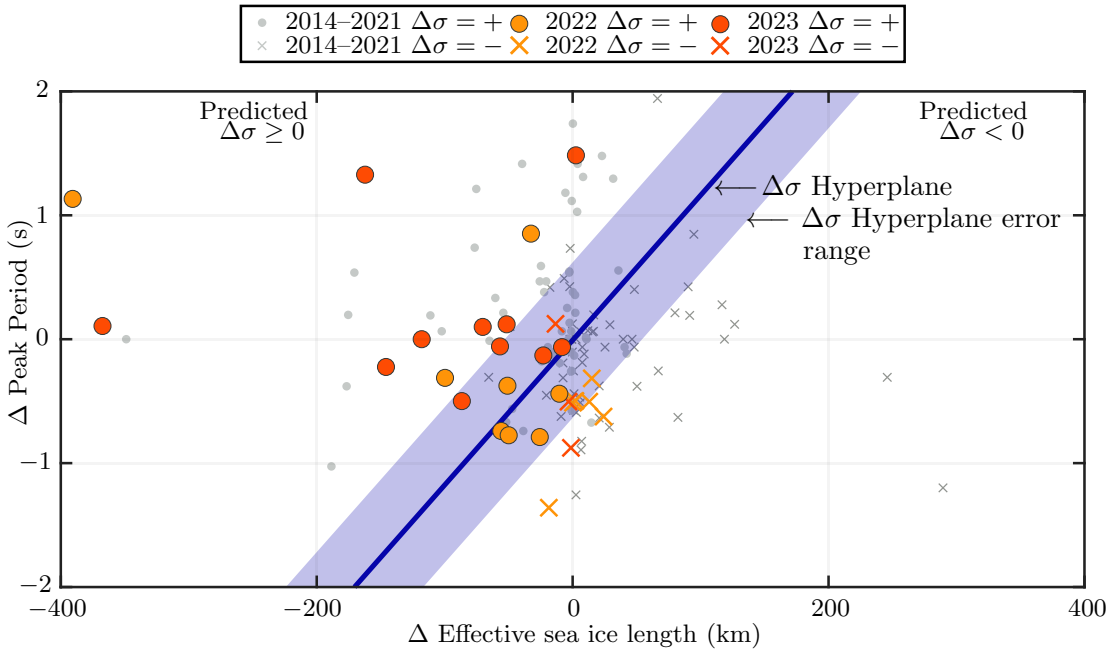

Figure 11. Support vector machine analysis of changes in flexural stress ($\Delta\sigma$) in relation to changes in 10th percentile effective sea-ice length and 90th percentile peak period for January–April over 2014–2021, expressed in terms of a hyperplane for predicted $\Delta\sigma = 0$ (blue line) and an error range (shaded blue region). Underlying yearly data points for each ice shelf over 2014–20921 are shown (grey markers), divided into predictions where $\Delta\sigma \geq 0$ (bullets) and $\Delta\sigma < 0$ (crosses). Corresponding data points are shown for 2022 (dark yellow) and 2023 (orange), also divided into $\Delta\sigma \geq 0$ (bullets) and $\Delta\sigma < 0$ (crosses).

3.4 Future scenarios

Most of the studied ice shelves experience large increases in flexural stress in 2022 and/or 2023 (Table 2). However, only a few reach flexural stress levels that are likely to be comparable to internal ice shelf stresses, which is predominantly because their shelf fronts are thick enough to reflect incoming swell (cf. Fig. 4). Following the thinning rates of Mertz, Pine Island and Thwaites (not shown), consider a future scenario where each shelf front thins by 1% per year from 2023 onwards, and how long it takes for the swell-induced flexural stress to reach 10 kPa in this scenario (an estimate for how much swell-induced flexural stress is required to match internal stress for a thin ice shelf; Bassis et al., 2024).

Coupled with the 1% shelf front thinning rate, consider the scenario in which the medians of the daily effective sea-ice lengths over 2022–2023 (January–April) for each ice shelf persist, and the incoming swell are based on the statistics of the incom-

https://doi.org/10.5194/egusphere-2026-3544
Preprint. Discussion started: 9 July 2026

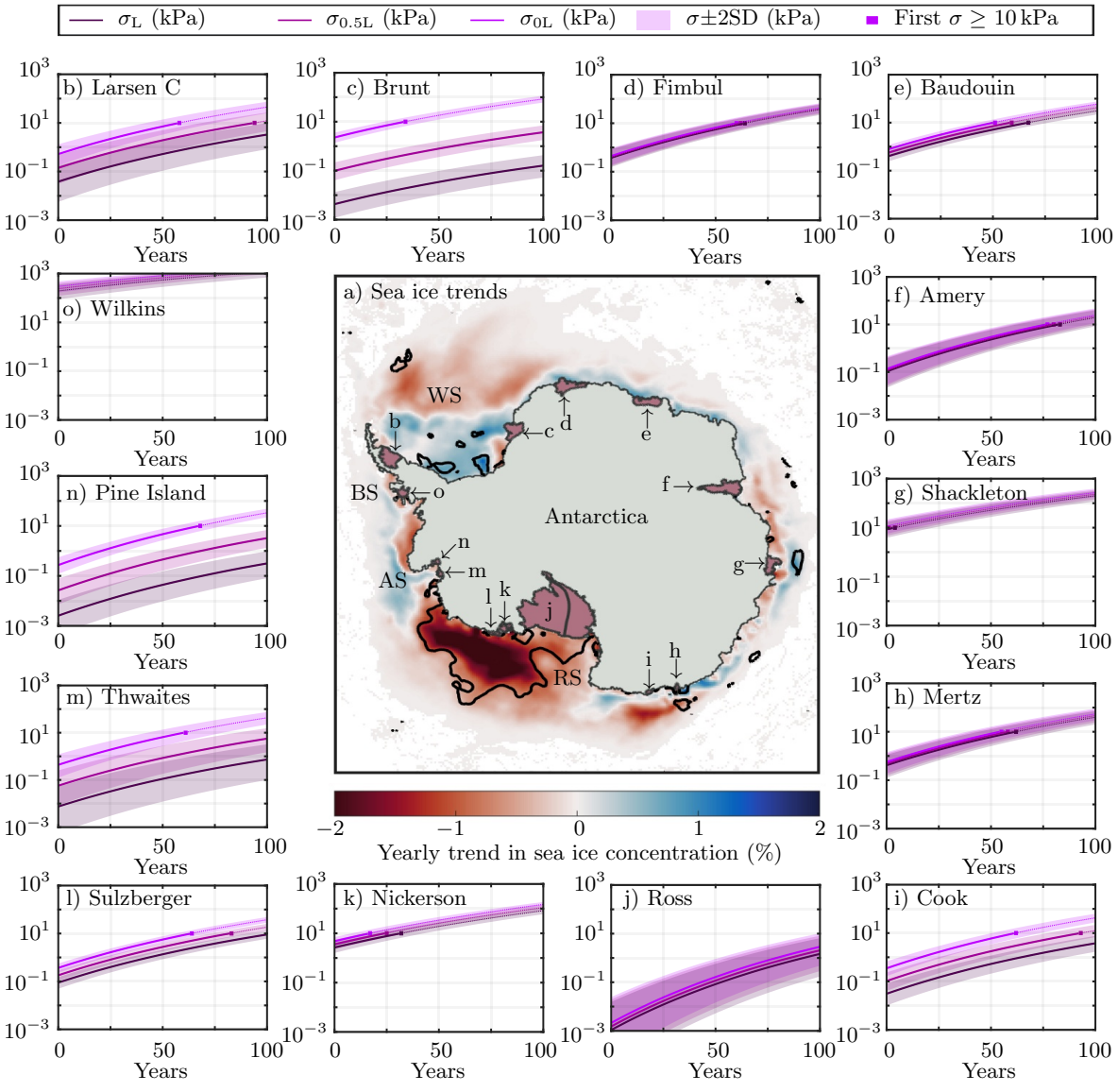

Figure 12. a) Sea ice concentration trends from 2000–2023 over January–April, with contours showing areas of statistically significant trends. b–o) Flexural stress for each of the 14 ice shelves over a hypothetical future 100 years, where the shelf fronts thin by 1% per year, with effective sea-ice lengths taken to be the medians of the respective 2022–2023 values (σ_L, dark purple), half the median 2022–2023 values ($\sigma_{0.5L}$, mid purple) and zero (σ_{0L}, light purple), and incoming significant wave heights and peak periods taken from the respective 2014–2023 values for each shelf (medians represented by lines and interquartile ranges by shading). The years in which the median flexural stress values exceed 10 kPa are indicated (dots). Sea ice data was taken from the NOAA/NSIDC Climate Data Record of Passive Microwave Sea Ice Concentration, Version 5.

https://doi.org/10.5194/egusphere-2026-3544
Preprint. Discussion started: 9 July 2026

ing swell from 2014–2023, where values of significant wave height and peak period are tested over the interquartile ranges (Fig. 12b–o, dark purple curves and shading). In this scenario, the coupled model predicts that seven of the ice shelves reach the 10 kPa threshold within 100 years (Fimbul, Baudouin, Amery, Shackleton, Mertz, Nickerson, Sulzberger, discounting Wilkins, which already has stress levels > 10 kPa; Fig. 12d–h,k,l), although Sulzberger only reaches the threshold for incoming swell near the upper bound of the interquartile range and Amery does not reach the threshold towards the lower bound of the range. Shackleton takes the shortest number of years to reach the threshold and Nickerson the second shortest, requiring only five and 33 years for their median values to exceed 10 kPa, respectively.

Based on the present trends in Antarctic sea ice in January–April (see Fig. 12a), there is the potential for sea-ice barriers to weaken in the future. Thus, consider the scenario where effective sea-ice lengths are half those in 2022–2023 (Fig. 12b–o, mid-purple curves and shading). The seven ice shelves that reached 10 kPa in the previous scenario (Fimbul, Baudouin, Amery, Shackleton, Mertz, Nickerson, Sulzberger) see a decrease by 2–20 years in the time required to reach the 10 kPa threshold (Fig. 12d–h,k,l). Larsen C and Cook also reach the threshold at their median values within 100 years in this scenario (Fig. 12b,i), i.e., nine of the 14 ice shelves are likely to have stress levels > 10 kPa.

In the scenario where the sea-ice barriers are completely lost ($L_{\text{eff}} = 0$), all studied ice shelves except Ross reach the 10 kPa threshold within 100 years and across the full interquartile ranges of incoming swell (Fig. 12b–o, light-purple curves and shading). Eight of the ice shelves (Larsen C, Fimbul, Baudouin, Mertz, Cook, Sulzberger, Thwaites, Pine Island) take between 50–70 years to reach the threshold at the median values of incoming swell. Even at the lowest end of the interquartile range, Shackleton reaches the threshold after 15 years and Nickerson after < 30 years.

4 Conclusions

Daily time series have been constructed for the flexural stress imposed on 14 Antarctic ice shelves, using effective lengths of sea-ice barriers surrounding the ice shelves and the significant wave heights and peak periods of incoming swell. They cover a decade leading up to and including the record Antarctic sea-ice minima of 2022 and 2023 (i.e., 2014–2023), constrained to months when ice shelves are most likely to be impacted by incoming swell (January–April). Results showed that flexural stress levels were generally much greater in 2022 and 2023 than the prior eight years (2014–2021). The increased flexural stress levels were attributed to reductions in effective sea-ice lengths in 2022 and 2023, but reductions in the peak periods of incoming swell were found to mitigate the increased stress and sometimes lead to decreased stress levels, particularly for East Antarctic ice shelves in 2022. Motivated by these initial findings, strong correlations were shown to exist between flexural stress anomalies and anomalies in effective sea-ice length and incoming swell peak period. Further, it shown that increases or decreases in flexural stress could be predicted with reasonable accuracy from knowledge of relative changes in effective sea-ice length and peak period.

https://doi.org/10.5194/egusphere-2026-3544
Preprint. Discussion started: 9 July 2026

To facilitate the study of 14 ice shelves over a decade, the daily time series of sea-ice length and incoming swell were constrained to chosen statistical levels. Thus, the incoming swell and sea ice data used may not be spatially or temporally aligned, adding some uncertainty to the results. Ongoing efforts to integrate swell propagation through sea ice into global wave and sea ice numerical models (Bennetts et al., 2017; Roach et al., 2019; Boutin et al., 2020) may partially reduce the uncertainty, by empowering hindcasts that predict swell reaching Antarctic ice shelves rather than just the sea ice edge. The model developments are complemented by the emergence of large-scale analysis of satellite altimetry observations of swell propagation into Antarctic sea ice (Fraser et al., 2026). Contemporary global wave models have not incorporated swell propagation into ice shelf/cavity regions, though recent developments in numerical methods may provide the basis for this extension, potentially within the next decade (Tazhimbetov et al., 2023; Papathanasiou et al., 2026).

In summary, we have conducted the broadest study to date on the impacts of ocean swell on Antarctic ice shelves, in terms of the number of ice shelves and length of the study period. We used data and models to quantify the major amplifications in flexural stress that Antarctic ice shelves experienced in the pronounced sea ice loss years of 2022 and 2023. If sea ice loss and ice shelf thinning continue, we predicted that many of the ice shelves will reach damaging flexural stress levels within the next century, and certain ice shelves, most notably Shackleton and Nickerson, are susceptible within a few decades. Thus, the study adds further evidence that changes in sea ice and ocean swell should be considered in future projections for Antarctic ice shelves.

Acknowledgements

The work was supported by the Australian Antarctic Science Program (Project 4528). NJT is funded by an Australian Government Research Training Program Scholarship administered by the University of Adelaide. LBG is supported by the Australian Research Council (ARC) grant DP240100325. LGB is supported by ARC grants FT190100404, DP200102828. PAR was supported through the Australian Bureau of Meteorology, and RAM the Australian Antarctic Division. RAM is supported by the ARC Special Research Initiative the Australian Centre for Excellence in Antarctic Science (SR200100008). The work of PAR and RAM contributes to the Australian Government's Australian Antarctic Partnership Program (AAPP). This project received grant funding from the Australian Government as part of the Antarctic Science Collaboration Initiative program. We would like to acknowledge Christan Melshiemer, Gunnar Spreen, Laurie Padman, Loren Carrère, Florent Lyard, European Space Agency, USGS, CSIRO and BoM for making the AMSR-E ARTIST ASI sea-ice concentration, CAWCR ocean hindcast data, Cryosat-2 ice elevations and the corrections to elevation data freely available, alongside Chris Stokes and one anonymous reviewer who gave helpful feedback for this work as part of the review process for my Ph.D. thesis.

https://doi.org/10.5194/egusphere-2026-3544
Preprint. Discussion started: 9 July 2026

Data and Code Availability

All codes will be made available on the Australian Antarctic Research Division data repository which will be made public upon manuscript acceptance. All data used in this project is freely available, with Daily AMSR2 ASI sea-ice concentration for Antarctica is available from https://data.seaice.uni-bremen.de/. Cryosat-2 ice elevation dataset is available from ftp://science-pds.cryosat.esa.int/. CAWCR hindcast data is available from https://data-cbr.csiro.au/thredds/catalog/catch_all/CMAR_CAWCR-Wave_archive/CAWCR_Wave_Hindcast_aggregate/catalog.html. Locations used for masking the locations of each ice shelf are available from Greene et al. (2022). For Figure 12, NOAA/NSIDC Climate Data Record of Passive Microwave Sea Ice Concentration, Version 5 is available from https://nsidc.org/data/g02202/versions/5.

Author Contributions

NJT and LGB conceptualized the study, alongside producing the images and writing the draft. NJT was responsible for data curation, analysis and methodology. LGB, PAR, and RAM provided supervision for NJT. LGB, PAR, and RAM obtained funding for this project. All authors contributed to reviewing and editing the writing, and approved the article for submission.

Competing Interests

The authors declare no competing interests.

https://doi.org/10.5194/egusphere-2026-3544
Preprint. Discussion started: 9 July 2026

References

Baker, M. G., Aster, R. C., Anthony, R. E., Chaput, J., Wiens, D. A., Nyblade, A., Bromirski, P. D., Gerstoft, P., and Stephen, R. A.: Seasonal and spatial variations in the ocean-coupled ambient wavefield of the Ross Ice Shelf, Journal of Glaciology, 65, 912–925, https://doi.org/10.1017/jog.2019.64, 2019.

Banwell, A. F., Willis, I. C., MacDonald, G. J., Goodsell, B., Mayer, D. P., Powell, A., and MacAyeal, D. R.: Calving and rifting on the McMurdo Ice Shelf, Antarctica, Annals of Glaciology, 58, 78–87, https://doi.org/10.1017/aog.2017.12, 2017.

Bassis, J. N., Crawford, A., Kachuck, S. B., Benn, D. I., Walker, C., Millstein, J., Duddu, R., Åström, J., Fricker, H. A., and Luckman, A.: Stability of Ice Shelves and Ice Cliffs in a Changing Climate, Annual Review of Earth and Planetary Sciences, 52, 221–247, https://doi.org/10.1146/annurev-earth-040522-122817, 2024.

Bennetts, L. G.: Waves in ice, in: Reference Module in Earth Systems and Environmental Sciences, Elsevier, https://doi.org/10.1016/B978-0-323-85242-5.00037-3, 2025.

Bennetts, L. G. and Squire, V. A.: Model sensitivity analysis of scattering-induced attenuation of ice-coupled waves, Ocean Modelling, 45, 1–13, https://doi.org/10.1016/j.ocemod.2012.01.002, 2012a.

Bennetts, L. G. and Squire, V. A.: On the calculation of an attenuation coefficient for transects of ice-covered ocean, Proceedings of the Royal Society A, 468, 136–162, https://doi.org/10.1098/rspa.2011.0155, 2012b.

Bennetts, L. G., O'Farrell, S., and Uotila, P.: Impacts of ocean-wave-induced breakup of Antarctic sea ice via thermodynamics in a stand-alone version of the CICE sea-ice model, The Cryosphere, 11, 1035–1040, https://doi.org/10.5194/tc-11-1035-2017, 2017.

Bennetts, L. G., Liang, J., and Pitt, J. P.: Modeling ocean wave transfer to Ross Ice Shelf flexure, Geophysical Research Letters, 49, e2022GL100 868, 2022.

Bennetts, L. G., Shakespeare, C. J., Vreugdenhil, C. A., Foppert, A., Gayen, B., Meyer, A., Morrison, A. K., Padman, L., Phillips, H. E., Stevens, C. L., et al.: Closing the loops on Southern Ocean dynamics: From the circumpolar current to ice shelves and from bottom mixing to surface waves, Reviews of Geophysics, 62, e2022RG000 781, 2024a.

Bennetts, L. G., Williams, T. D., and Porter, R.: A thin-plate approximation for ocean wave interactions with an ice shelf, Journal of Fluid Mechanics, 984, A48, https://doi.org/10.1017/jfm.2024.200, 2024b.

Bindschadler, R., Choi, H., Wichlacz, A., Bingham, R., Bohlander, J., Brunt, K., Corr, H., Drews, R., Fricker, H., Hall, M., et al.: Getting around Antarctica: new high-resolution mappings of the grounded and freely-floating boundaries of the Antarctic ice sheet created for the International Polar Year, The Cryosphere, 5, 569–588, 2011.

Boutin, G., Lique, C., Ardhuin, F., Rousset, C., Talandier, C., Accensi, M., and Girard-Ardhuin, F.: Towards a coupled model to investigate wave–sea ice interactions in the Arctic marginal ice zone, The Cryosphere, 14, 709–735, https://doi.org/10.5194/tc-14-709-2020, 2020.

Carrère, L. and Lyard, F.: Modeling the barotropic response of the global ocean to atmospheric wind and pressure forcing - Comparisons with observations, Geophysical Research Letters, 30, 1–4, https://doi.org/10.1029/2002GL016473, 2003.

Chuter, S. J. and Bamber, J. L.: Antarctic ice shelf thickness from CryoSat-2 radar altimetry, Geophysical Research Letters, 42, 10 721–10 729, https://doi.org/10.1002/2015GL066515, 2015.

Davison, B. J., Hogg, A. E., Gourmelen, N., Jakob, L., Wuite, J., Nagler, T., Greene, C. A., Andreasen, J., and Engdahl, M. E.: Annual mass budget of Antarctic ice shelves from 1997 to 2021, Science Advances, 9, 1–12, https://doi.org/10.1126/sciadv.adi0186, 2023.

https://doi.org/10.5194/egusphere-2026-3544
Preprint. Discussion started: 9 July 2026

Day, N. S., Bennetts, L. G., O'Farrell, S. P., Alberello, A., and Montiel, F.: Analysis of the Antarctic marginal ice zone based on unsupervised classification of standalone sea ice model data, Journal of Geophysical Research: Oceans, 129, 1–19, https://doi.org/10.1029/2024JC020953, 2024.

Doddridge, E. W., Hobbs, W., Auger, M., Boyd, P. W., Chua, S. M. T., Cook, S., Corney, S., Emmerson, L., Fraser, A. D., Heil, P., Kelly, N., Lannuzel, D., Li, X., Liniger, G., Massom, R. A., Meyer, A., Reid, P., Southwell, C., Spence, P., Steketee, A., Swadling, K. M., Teder, N., Wienecke, B., Wongpan, P., and Yamazaki, K.: Impacts of Antarctic summer sea-ice extremes, PNAS Nexus, 4, https://doi.org/10.1093/pnasnexus/pgaf164, 2025.

Eayrs, C., Li, X., Raphael, M. N., and Holland, D. M.: Rapid decline in Antarctic sea ice in recent years hints at future change, Nature Geoscience, 14, 460–464, https://doi.org/10.1038/s41561-021-00768-3, 2021.

Francis, D., Fonseca, R., Mattingly, K. S., Marsh, O. J., Lhermitte, S., and Cherif, C.: Atmospheric triggers of the Brunt Ice Shelf calving in February 2021, Journal of Geophysical Research: Atmospheres, 127, 1–15, https://doi.org/10.1029/2021JD036424, 2022.

Fraser, A. D., Day, N. S., Wang, Z., Bennetts, L. G., Liu, Q., O'Farrell, S., Coleman, R., Voermans, J., Xu, S., Zhu, W., Auger, M., Massom, R. A., Wongpan, P., Craw, L., Brouwer, J., Toyota, T., Heil, P., and Horvat, C.: Revealing the Antarctic marginal ice zone: a decade-long wave-in-ice climatology, Nature Communications, https://doi.org/https://doi.org/10.1038/s41467-026-73203-z, 2026.

Fretwell, P., Pritchard, H. D., Vaughan, D. G., Bamber, J. L., Barrand, N. E., Bell, R., Bianchi, C., Bingham, R. G., Blankenship, D. D., Casassa, G., Catania, G., Callens, D., Conway, H., Cook, A. J., Corr, H. F., Damaske, D., Damm, V., Ferraccioli, F., Forsberg, R., Fujita, S., Gim, Y., Gogineni, P., Griggs, J. A., Hindmarsh, R. C., Holmlund, P., Holt, J. W., Jacobel, R. W., Jenkins, A., Jokat, W., Jordan, T., King, E. C., Kohler, J., Krabill, W., Riger-Kusk, M., Langley, K. A., Leitchenkov, G., Leuschen, C., Luyendyk, B. P., Matsuoka, K., Mouginot, J., Nitsche, F. O., Nogi, Y., Nost, O. A., Popov, S. V., Rignot, E., Rippin, D. M., Rivera, A., Roberts, J., Ross, N., Siegert, M. J., Smith, A. M., Steinhage, D., Studinger, M., Sun, B., Tinto, B. K., Welch, B. C., Wilson, D., Young, D. A., Xiangbin, C., and Zirizzotti, A.: Bedmap2: Improved ice bed, surface and thickness datasets for Antarctica, The Cryosphere, 7, 375–393, https://doi.org/10.5194/tc-7-375-2013, 2013.

Fürst, J. J., Durand, G., Gillet-Chaulet, F., Tavard, L., Rankl, M., Braun, M., and Gagliardini, O.: The safety band of Antarctic ice shelves, Nature Climate Change, 6, 479–482, https://doi.org/10.1038/nclimate2912, 2016.

Gilbert, E. and Holmes, C.: 2023's Antarctic sea ice extent is the lowest on record, Weather, 79, 46–51, https://doi.org/10.1002/wea.4518, 2024.

Golden, K. M., Bennetts, L. G., Cherkaev, E., Eisenman, I., Feltham, D., Horvat, C., Hunke, E., Jones, C., Perovich, D. K., Ponte-Castaneda, P., Strong, C., Sulsky, D., and Wells, A. J.: Modeling sea ice, Notices of the American Mathematical Society, 67, 1535–1555, https://doi.org/0.1090/noti2171, 2020.

Gomez-Fell, R., Wolfgang, R., Purdie, H., and Marsh, O.: Parker Ice Tongue collapse, Antarctica, triggered by loss of stabilizing land-fast sea ice, Geophysical Research Letters, 49, 1–11, https://doi.org/10.1029/2021GL096156, 2022.

Greene, C. A., Gardner, A. S., Schlegel, N., and Fraser, A. D.: Antarctic calving loss rivals ice-shelf thinning, Nature, 609, 948–953, https://doi.org/10.1038/s41586-022-05037-w, 2022.

Gudmundsson, G. H.: Ice-shelf buttressing and the stability of marine ice sheets, Cryosphere, 7, 647–655, https://doi.org/10.5194/tc-7-647-2013, 2013.

Gulev, S. K., Thorne, P., Ahn, J., Dentener, F. J., Domingues, C. M., Gerland, S., Gong, D., Kaufman, D., Nnamchi, H., Quaas, J., Rivera, J., Sathyendranath, S., Smith, S., Trewin, B., von Schuckmann, K., and Vose, R.: 2021: Changing State of the Climate System. In Climate Change 2021: The Physical Science Basis. Contribution of Working Group I to the Sixth Assessment Report of the Intergovernmental

https://doi.org/10.5194/egusphere-2026-3544
Preprint. Discussion started: 9 July 2026

Panel on Climate Change [Masson-Delmotte, V., P. Zhai, A. Pirani, S.L. Connors, C. Péan, S. Berger, N. Caud, Y. Chen, L. Goldfarb, M.I. Gomis, M. Huang, K. Leitzell, E. Lonnoy, J.B.R. Matthews, T.K. Maycock, T. Waterfield, O. Yelekçi, R. Yu, and B. Zhou (eds.)], Cambridge University Press, Cambridge, United Kingdom and New York, NY, USA,, https://doi.org/10.1017/9781009157896.004, 2021.

Hobbs, W., Spence, P., Meyer, A., Schroeter, S., Fraser, A. D., Reid, P., Tian, T. R., Wang, Z., Liniger, G., Doddridge, E. W., et al.: Observational evidence for a regime shift in summer Antarctic sea ice, Journal of Climate, 37, 2263–2275, 2024.

Hogg, A. E. and Gudmundsson, G. H.: Commentary: Impacts of the Larsen-C Ice Shelf calving event, Nature Climate Change, 7, 540–542, https://doi.org/10.1038/nclimate3359, 2017.

Kurtz, N. T. and Markus, T.: Satellite observations of Antarctic sea ice thickness and volume, Journal of Geophysical Research: Oceans, 117, 1–9, 2012.

Liang, J., Pitt, J. P. A., and Bennetts, L. G.: Pan-Antarctic assessment of ice shelf flexural responses to ocean waves, Journal of Geophysical Research: Oceans, 129, 1–16, https://doi.org/10.1029/2023JC020824, 2024.

Ligtenberg, S. R., Kuipers Munneke, P., and Van Den Broeke, M. R.: Present and future variations in Antarctic firn air content, The Cryosphere, 8, 1711–1723, https://doi.org/10.5194/tc-8-1711-2014, 2014.

Lipovsky, B. P.: Ice Shelf Rift Propagation and the Mechanics of Wave-Induced Fracture, Journal of Geophysical Research: Oceans, 123, 4014–4033, https://doi.org/10.1029/2017JC013664, 2018.

Liu, J., Li, R., Li, S., Meucci, A., and Young, I. R.: Increasing wave power due to global climate change and intensification of Antarctic Oscillation, Applied Energy, 358, 122 572, https://doi.org/doi.org/10.1016/j.apenergy.2023.122572, 2024.

Lyard, F., Lefevre, F., Letellier, T., and Francis, O.: Modelling the global ocean tides: Modern insights from FES2004, Ocean Dynamics, 56, 394–415, https://doi.org/10.1007/s10236-006-0086-x, 2006.

Marsh, O. J., Luckman, A. J., and Hodgson, D. A.: Rapid acceleration of the Brunt Ice Shelf after calving of iceberg A-81, The Cryosphere, 18, 705–710, https://doi.org/10.5194/tc-18-705-2024, 2024.

Massom, R. A., Giles, A. B., Fricker, H. A., Warner, R. C., Legrésy, B., Hyland, G., Young, N., and Fraser, A. D.: Examining the interaction between multi-year landfast sea ice and the Mertz Glacier Tongue, East Antarctica: Another factor in ice sheet stability?, Journal of Geophysical Research: Oceans, 115, 1–15, https://doi.org/10.1029/2009JC006083, 2010.

Massom, R. A., Scambos, T. A., Bennetts, L. G., Reid, P., Squire, V. A., and Stammerjohn, S. E.: Antarctic ice shelf disintegration triggered by sea ice loss and ocean swell, Nature, 558(7710), 383–389, https://doi.org/10.1038/s41586-018-0212-1, 2018.

Meier, W. N., Stewart, J. S., Liu, Y., Key, J., and Miller, J. A.: Operational Implementation of Sea Ice Concentration Estimates from the AMSR2 Sensor, IEEE Journal of Selected Topics in Applied Earth Observations and Remote Sensing, 10, 3904–3911, https://doi.org/10.1109/JSTARS.2017.2693120, 2017.

Meylan, M. H., Ilyas, M., Lamichhane, B. P., and Bennetts, L. G.: Swell-induced flexural vibrations of a thickening ice shelf over a shoaling seabed, Proceedings of the Royal Society A, 477, 1–20, https://doi.org/10.1098/rspa.2021.0173, 2021.

Mouginot, J., Scheuchl, B., and Rignot, E.: MEaSUREs Antarctic Boundaries for IPY 2007-2009 from Satellite Radar, Version 2., https://doi.org/10.5067/AXE4121732AD., 2017.

Noble, T. L. et al.: The sensitivity of the Antarctic Ice Sheet to a changing climate, Reviews of Geophysics, 58, e2019RG000 663, 2020.

Padman, L., Fricker, H. A., Coleman, R., Howard, S., and Erofeeva, L.: A new tide model for the Antarctic ice shelves and seas, Annals of Glaciology, 34, 247–254, https://doi.org/10.3189/172756402781817752, 2002.

Papathanasiou, T. K., Bennetts, L. G., and Meylan, M. H.: Modelling hydroelastic flexure of arbitrarily shaped ice shelves forced by long ocean waves, arXiv preprint xxxx.7617646, 2026.

https://doi.org/10.5194/egusphere-2026-3544
Preprint. Discussion started: 9 July 2026

Parkinson, C. L.: A 40-y record reveals gradual Antarctic sea ice increases followed by decreases at rates far exceeding the rates seen in the Arctic, Proceedings of the National Academy of Sciences of the United States of America, 116, 14 414–14 423, https://doi.org/10.1073/pnas.1906556116, 2019.

Provost, F., Zigone, D., Le Meur, E., Malet, J.-P., and Hibert, C.: Surface dynamics and history of the calving cycle of Astrolabe Glacier (Adélie Coast, Antarctica) derived from satellite imagery, The Cryosphere, 18, 3067–3079, 2024.

Purich, A. and Doddridge, E. W.: Record low Antarctic sea ice coverage indicates a new sea ice state, Communications Earth and Environment, 4, 1–9, https://doi.org/10.1038/s43247-023-00961-9, 2023.

Qi, M., Liu, Y., Liu, J., Cheng, X., Lin, Y., Feng, Q., Shen, Q., and Yu, Z.: A 15-year circum-Antarctic iceberg calving dataset derived from continuous satellite observations, Earth System Science Data, 13, 4583–4601, https://doi.org/10.5194/essd-13-4583-2021, 2021.

Reid, P., Stammerjohn, S., Massom, R., Scambos, T., and Lieser, J.: The record 2013 Southern Hemisphere sea-ice extent maximum, Annals of Glaciology, 56, 99–106, https://doi.org/10.3189/2015AoG69A892, 2015.

Reid, P. A. and Massom, R. A.: Successive Antarctic sea ice extent records during 2012, 2013 and 2014, In: State of the Climate in 2014. , Special Supplement to the Bulletin of the American Meteorological Society, 96, 7, https://doi.org/10.1175/2015BAMSStateoftheClimate.1, 2015.

Reid, P. A., Stammerjohn, S., Massom, R. A., Barreira, S., Scambos, T. A., and Lieser, J. L.: Sea-ice extent, concentration, and seasonality [in "State of the Climate in 2023"], Bulletin of the American Meteorological Society, 105, S343–S345, https://doi.org/10.1175/BAMS-D-24-0099.1, 2024.

Roach, L. A., Bitz, C. M., Horvat, C., and Dean, S. M.: Advances in modeling interactions between sea ice and ocean surface waves, Journal of Advances in Modeling Earth Systems, 11, 4167–4181, 2019.

Schroeter, S., O'Kane, T. J., and Sandery, P. A.: Antarctic sea ice regime shift associated with decreasing zonal symmetry in the Southern Annular Mode, Cryosphere, 17, 701–717, https://doi.org/10.5194/tc-17-701-2023, 2023.

Siegfried, M. R., Fricker, H. A., Roberts, M., Scambos, T. A., and Tulaczyk, S.: A decade of West Antarctic subglacial lake interactions from combined ICESat and CryoSat-2 altimetry, Geophysical Research Letters, 41, 891–898, https://doi.org/10.1002/2013GL058616, 2014.

Smith, G. A., Hemer, M., Greenslade, D., Trenham, C., Zieger, S., and Durrant, T.: Global wave hindcast with Australian and Pacific Island focus: From past to present, Geoscience Data Journal, 8, 1–10, https://doi.org/10.1002/gdj3.104, 2020.

Squire, V. A.: Ocean Wave Interactions with Sea Ice: A Reappraisal, Annual Review of Fluid Mechanics, 52, 37–60, https://doi.org/10.1146/annurev-fluid-010719-060301, 2020.

Tazhimbetov, N., Almquist, M., Werpers, J., and Dunham, E. M.: Simulation of flexural-gravity wave propagation for elastic plates in shallow water using an energy-stable finite difference method with weakly enforced boundary and interface conditions, Journal of Computational Physics, 493, 112 470, https://doi.org/10.1016/j.jcp.2023.112470, 2023.

Teder, N. J., Bennetts, L. G., Reid, P. A., and Massom, R. A.: Sea ice-free corridors for large swell to reach Antarctic ice shelves, Environmental Research Letters, 17, 1–11, https://doi.org/10.1088/1748-9326/ac5edd, 2022.

Teder, N. J., Bennetts, L. G., Reid, P. A., Massom, R. A., Pitt, J. P. A., Scambos, T. . A., and Fraser, A. D.: Large-scale ice-shelf calving events follow prolonged amplifications in flexure, Nature Geoscience, 18, 599–606, https://doi.org/10.1038/s41561-025-01713-4, 2025.

Tolman, H. L.: Treatment of unresolved islands and ice in wind wave models, Ocean Modelling, 5, 219–231, https://doi.org/S1463-5003(02)00040-9, 2003.

Turner, J., Holmes, C., Harrison, T. C., Phillips, T., Jena, B., Reeves-Francois, T., Fogt, R., Thomas, E. R., and Bajish, C. C.: Record Low Antarctic Sea Ice Cover in February 2022, Geophysical Research Letters, 49, 1–12, https://doi.org/10.1029/2022GL098904, 2022.

https://doi.org/10.5194/egusphere-2026-3544
Preprint. Discussion started: 9 July 2026

Walker, C. C., Millstein, J. D., Miles, B. W. J., Cook, S., Fraser, A. D., Colliander, A., Misra, S., Trusel, L. D., Adusumilli, S., Roberts, C., and Fricker, H. A.: Multi-decadal collapse of East Antarctica's Conger–Glenzer Ice Shelf, Nature Geoscience, 17, 1240–1248, https://doi.org/10.1038/s41561-024-01582-3, 2024.

Wang, S., Liu, J., Cheng, X., Yang, D., Kerzenmacher, T., Li, X., Hu, Y., and Braesicke, P.: Contribution of the deepened Amundsen Sea Low to the record low Antarctic sea ice extent in February 2022, Environmental Research Letters, 18, 054 002, 2023.

Williams, T. D., Bennetts, L. G., Squire, V. A., Dumont, D., and Bertino, L.: Wave-ice interactions in the marginal ice zone. Part 1: Theoretical foundations, Ocean Modelling, 71, 81–91, https://doi.org/10.1016/j.ocemod.2013.05.010, 2013a.

Williams, T. D., Bennetts, L. G., Squire, V. A., Dumont, D., and Bertino, L.: Wave-ice interactions in the marginal ice zone. Part 2: Numerical implementation and sensitivity studies along 1D transects of the ocean surface, Ocean Modelling, 71, 92–101, https://doi.org/10.1016/j.ocemod.2013.05.011, 2013b.

Young, I. R., Fontaine, E., Liu, Q., and Babanin, A. V.: The wave climate of the Southern Ocean, Journal of Physical Oceanography, 50, 1417–1433, https://doi.org/10.1175/JPO-D-20-0031.1, 2020.

Zhao, A., Cheng, Y., Fraser, A. D., Bennetts, L. G., Xiao, H., Liang, Q., Li, T., and Li, R.: Long-term evolution of the Sulzberger Ice Shelf, West Antarctica: Insights from 74-year observations and 2022 Hunga-Tonga volcanic tsunami-induced calving, Earth and Planetary Science Letters, 646, 1–13, https://doi.org/10.1016/j.epsl.2024.118958, 2024.

Zwally, H. J.: Variability of Antarctic sea ice 1979–1998, Journal of Geophysical Research, 107, 3041, https://doi.org/10.1029/2000JC000733, 2002.